

ARTICLE

DOI: 10.1038/s41467-017-00215-1

OPEN

ROR α controls hepatic lipid homeostasis via negative regulation of PPAR γ transcriptional network

Kyeongkyu Kim¹, Kyungjin Boo¹, Young Suk Yu¹, Se Kyu Oh¹, Hyunkyung Kim¹, Yoon Jeon², Jinhyuk Bhin³, Daehee Hwang³, Keun Il Kim⁴, Jun-Su Lee⁵, Seung-Soon Im⁵, Seul Gi Yoon^{6,7}, Il Yong Kim^{6,7}, Je Kyung Seong^{6,7,8}, Ho Lee², Sungsoon Fang⁹ & Sung Hee Baek¹

The retinoic acid receptor-related orphan receptor- α (ROR α) is an important regulator of various biological processes, including cerebellum development, circadian rhythm and cancer. Here, we show that hepatic ROR α controls lipid homeostasis by negatively regulating transcriptional activity of peroxisome proliferators-activated receptor- γ (PPAR γ) that mediates hepatic lipid metabolism. Liver-specific *Rora*-deficient mice develop hepatic steatosis, obesity and insulin resistance when challenged with a high-fat diet (HFD). Global transcriptome analysis reveals that liver-specific deletion of *Rora* leads to the dysregulation of PPAR γ signaling and increases hepatic glucose and lipid metabolism. ROR α specifically binds and recruits histone deacetylase 3 (HDAC3) to PPAR γ target promoters for the transcriptional repression of PPAR γ . PPAR γ antagonism restores metabolic homeostasis in HFD-fed liver-specific *Rora* deficient mice. Our data indicate that ROR α has a pivotal role in the regulation of hepatic lipid homeostasis. Therapeutic strategies designed to modulate ROR α activity may be beneficial for the treatment of metabolic disorders.

¹Department of Biological Sciences, Creative Research Initiatives Center for Chromatin Dynamics, Seoul National University, Seoul 08826, South Korea. ²Graduate School of Cancer Science and Policy, Research Institute, National Cancer Center, Gyeonggi-do 10408, South Korea. ³Department of New Biology and Center for Plant Aging Research, Institute for Basic Science, DGIST, Daegu 42988, South Korea. ⁴Department of Biological Sciences, Sookmyung Women's University, Seoul 04310, South Korea. ⁵Department of Physiology, Keimyung University School of Medicine, Daegu 42601, South Korea. ⁶Laboratory of Developmental Biology and Genomics, College of Veterinary Medicine, Research Institute for Veterinary Science, Seoul National University, Seoul 08826, South Korea. ⁷Korea Mouse Phenotyping Center, Seoul 08826, South Korea. ⁸BK21 Plus Program for Creative Veterinary Science Research, BIO-MAX institute, Interdisciplinary Program for Bioinformatics and Program for Cancer Biology, Seoul National University, Seoul 08826, South Korea. ⁹Severance Biomedical Science Institute, BK21 Plus Project for Medical Science, Gangnam Severance Hospital, Yonsei University College of Medicine, Seoul 06273, South Korea. Kyeongkyu Kim and Kyungjin Boo contributed equally to this work. Correspondence and requests for materials should be addressed to S.F. (email: sfang@yuhs.ac) or to S.H.B. (email: sbaek@snu.ac.kr)

Obesity is a high-risk metabolic disorder, leading to various complications, including cardiovascular disease, hyperlipidemia and type II diabetes^{1–3}. Ectopic accumulation of fat in various tissues activates numerous cellular stress and inflammatory signaling pathways, resulting in insulin resistance, pancreatic β -cell dysfunction, and hepatic steatosis⁴. The liver is the central metabolic organ to regulate key aspects of glucose and lipid metabolism including gluconeogenesis, fatty acid β -oxidation, lipoprotein uptake and secretion and lipogenesis⁵. Given that portal vein is a critical path to convey insulin signaling from pancreas during fed state, the hepatic glucose and lipid metabolism are directly under control of nutrient signaling.

Dysregulation of hepatic lipid metabolism results in the development of hepatic steatosis, contributing to the chronic insulin resistance and steatotic hepatitis^{6,7}. The hepatic metabolic pathways are governed by highly dynamic transcriptional networks of orphan nuclear receptors (ONRs), including proliferator-activated receptor- γ (PPAR γ), farnesoid X receptor, and liver X receptor⁸. ONRs are ligand-activated transcription factors with no defined ligands^{9,10}. Many ONRs are expressed in tissues involved in metabolism, such as skeletal muscle, adipose tissue and liver^{11,12}, and play critical roles in the regulation of metabolism¹³. Genetic studies have shown that many ONRs regulate nutrient metabolism and physiology of obesity and type II diabetes^{14–16}. Given that numerous synthesized ligands for ONRs are used for developing putative drugs for human metabolic diseases^{17–19}, ONRs are emerging as therapeutic targets for the treatment of metabolic diseases.

Previously, we have reported that receptor-related orphan receptor- α (ROR α), a member of ONRs, possesses tumor suppressive function by transrepressing canonical Wnt/ β -catenin signaling leading to inhibition of colon cancer growth and by increasing p53 stability upon DNA damage response^{20,21}. ROR α is known to regulate cerebellum development²². The *staggerer* (*sg*) mice, natural *Rora* spontaneous mutant mice, display ataxia and severe cerebellar atrophy²³. Moreover, ROR α functions to regulate circadian rhythm as a key regulator of the cyclic expression of BMAL1 together with REV-ERB α ²⁴. The ROR α /REV-ERB α feedback loop controls the circadian expression pattern of BMAL1, indicating that ROR α plays a key role in the core circadian clock²⁵. In addition, *sg* mice show lower expression levels of genes involved in lipid metabolism, including apolipoprotein A-1 (*apoA1*) and apolipoprotein C-III (*apoCIII*)^{26,27}. Thus, *sg* mice exhibit less body weight gain compared with wild-type (WT) mice²⁸. Given that *sg* mice have huge cerebellar defects, it is still possible that physiological changes observed in *sg* mice are indirect effects. Thus, the physiological roles of ROR α to control transcriptional networks to modulate lipogenesis and gluconeogenesis still remain unclear.

Here, we report that ROR α plays a key role to control hepatic lipid metabolism to protect against diet-induced obesity and hepatic steatosis, using liver-specific *Rora*-deficient mouse model. High-fat diet (HFD)-fed liver-specific *Rora* deficient mice (ROR α ^{LKO} mice) show severe metabolic defects, including hepatic steatosis, obesity, and insulin resistance, although no physiological changes have been observed with control diet (CD). Genome-wide transcriptome analysis reveals that PPAR γ signaling is remarkably elevated in ROR α ^{LKO} mice. ROR α specifically recruits HDAC3 to the PPAR γ target promoters to suppress PPAR γ transcriptional activity. Finally, PPAR γ antagonism by using PPAR γ antagonist GW9662, largely ameliorates body weight gain and hepatic steatosis in HFD-fed ROR α ^{LKO} mice, indicating that dysregulated PPAR γ signaling is a critical metabolic cue, leading to metabolic defects in HFD-fed ROR α ^{LKO} mice. Together, our data demonstrate that ROR α

controls PPAR γ signaling to protect against hepatic metabolic homeostasis and obesity in response to HFD.

Results

HFD induces obesity in liver-specific *Rora*-deficient mice.

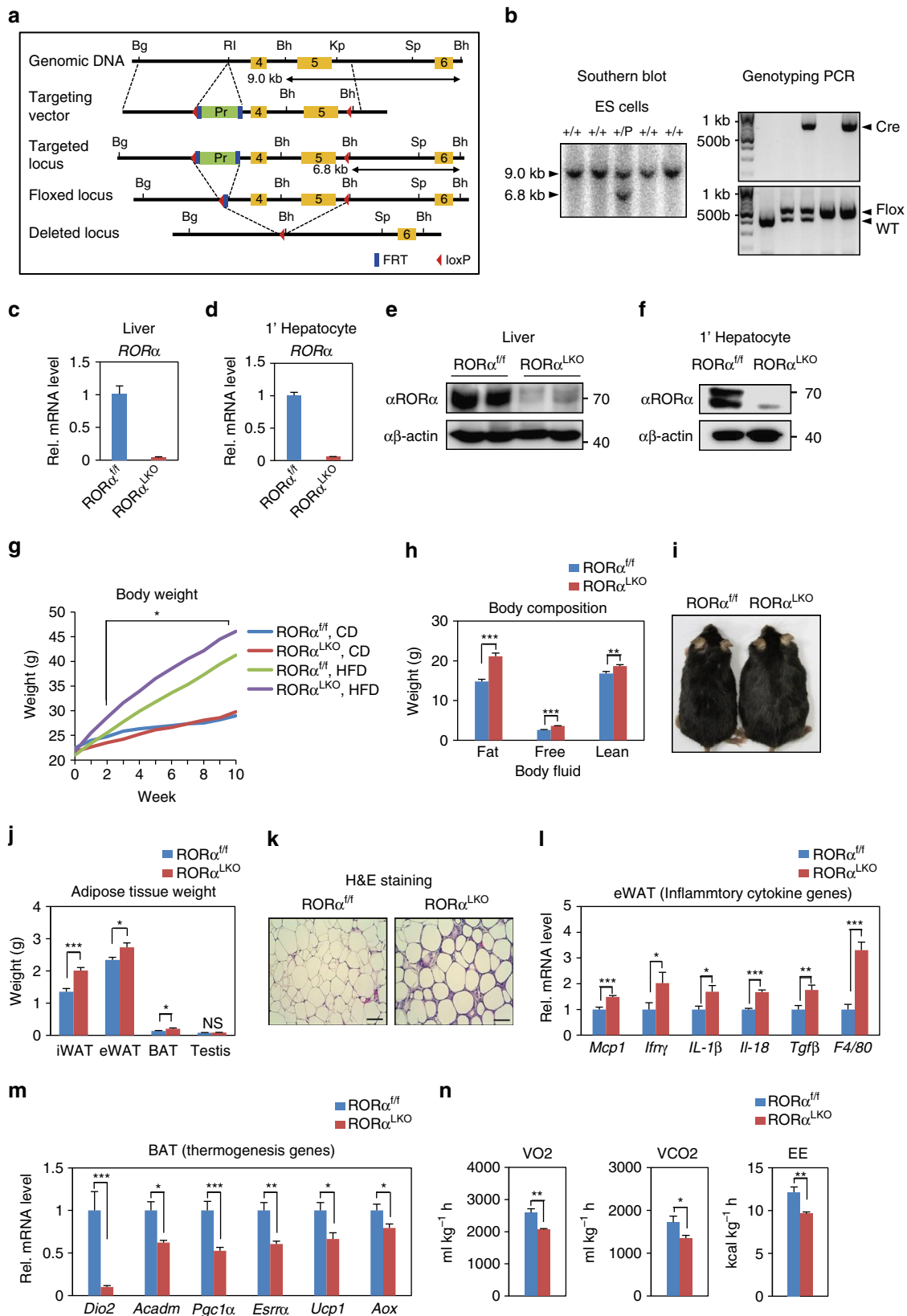
To determine the physiological roles of ROR α in the liver, we generated ROR α -floxed mice (ROR α ^{fl/f}) by gene targeting in ES cells and crossed ROR α floxed mice with Albumin-Cre (Alb-Cre) mice to selectively create liver-specific *Rora* conditional knockout (KO) mice (hereafter named ROR α ^{LKO}) (Fig. 1a, b). The mRNA and protein levels of endogenous hepatic ROR α were remarkably depleted in ROR α ^{LKO} mice compared with littermate controls (hereafter named ROR α ^{fl/f}) (Fig. 1c–f). We measured the growth rate of ROR α ^{LKO} mice and observed that they attained body weights similar to ROR α ^{fl/f} mice fed CD during 10 weeks from 8 weeks old (Fig. 1g). Body composition analysis revealed that ROR α ^{LKO} mice exhibited similar fat/lean mass, free body fluid and adipocytes size with those of ROR α ^{fl/f} (Supplementary Fig. 1a, b). However, when placed on a HFD, ROR α ^{LKO} mice exhibited a significant increase of the weight gain (20 vs. 25 g) compared with their ROR α ^{fl/f} littermates, resulting in extraordinary obesity (Fig. 1g). Body composition analysis and macroscopic view revealed that ROR α ^{LKO} mice had more fat mass (Fig. 1h, i). All white and brown fat depots from ROR α ^{LKO} mice were significantly increased in mass relative to ROR α ^{fl/f} (Fig. 1j). During obesity, adipose tissue expands by hyperplastic and/or hypertrophic growth. The cross-sectional area of adipocytes in visceral fat tissue was markedly increased in ROR α ^{LKO} mice compared with ROR α ^{fl/f} mice (Fig. 1k). Induction of pro-inflammatory genes, including *Mcp1*, *Ifny*, and *F4/80* in visceral fat depot were potentiated in ROR α ^{LKO} mice (Fig. 1l). Consistent with a significant weight gain in HFD-fed ROR α ^{LKO} mice, gene expression analysis revealed reduction of *Pgc1 α* , as well as a number of genes involved in thermogenesis, mitochondrial biogenesis, and fatty acid oxidation in brown adipose tissue of ROR α ^{LKO} mice compared with that of ROR α ^{fl/f} littermates (Fig. 1m). The observation that energy expenditure (EE) in brown fat has been impaired in HFD-fed ROR α ^{LKO} mice led us to examine whether they have global metabolic defects. Although no obvious defects were observed in mice on CD (Supplementary Fig. 1c), HFD-fed ROR α ^{LKO} mice were found to produce far less CO₂, consume less O₂ and expend less energy than ROR α ^{fl/f} littermates, indicating that oxidative phosphorylation is impaired by the hepatic deletion of ROR α (Fig. 1n and Supplementary Fig. 1d). Previously, bile acids have been reported to increase EE by promoting intracellular thyroid hormone activation in brown adipose tissue²⁹. We observed that expression of key genes involved in hepatic bile acid synthesis was remarkably reduced in HFD-fed ROR α ^{LKO} mice (Supplementary Fig. 1e). Consistently, serum bile acid pool sizes in HFD-fed ROR α ^{LKO} mice were markedly less than ROR α ^{fl/f} littermates (Supplementary Fig. 1f), implicating that reduction of bile acid synthesis and bile acid pool size led to reduced EE in brown adipose tissue of HFD-fed ROR α ^{LKO} mice.

Hepatic steatosis impairs insulin sensitivity in ROR α ^{LKO} mice.

Obesity is largely associated with hepatic steatosis in humans as well as in rodents. Consistent with obese phenotype in ROR α ^{LKO} mice, large lipid vesicles with increased amounts were observed in the hepatocytes of HFD-fed ROR α ^{LKO} mice (Fig. 2a). Macroscopically, liver from HFD-fed ROR α ^{LKO} mice was markedly enlarged and paler compared with HFD-fed ROR α ^{fl/f} liver (Fig. 2b). Consistently, HFD-fed ROR α ^{LKO} mice exhibited a remarkable increase of liver weight compared with HFD-fed ROR α ^{fl/f} mice (Fig. 2c). In accordance with hematoxylin and eosin

staining, oil red O staining and hepatic triglyceride (TG) analysis showed a dramatic increase in lipid level in the HFD-fed $ROR\alpha^{LKO}$ liver compared with the HFD-fed $ROR\alpha^{ff}$ liver, whereas no difference was observed in CD-fed $ROR\alpha^{ff}$ and $ROR\alpha^{LKO}$ mice (Fig. 2d, e and Supplementary Fig. 1g). While

hepatic gene expression profiles were similar among CD-fed genotypes (Supplementary Fig. 1h), hepatic gene expression profiles of lipogenesis, gluconeogenesis, and lipid sequestration in the HFD-fed $ROR\alpha^{LKO}$ were largely increased, indicating that $ROR\alpha$ protects against HFD-induced hepatic steatosis (Fig. 2f).



Obesity and hepatic steatosis often predispose rodents and humans to impaired glucose homeostasis and insulin resistance^{30–32}. Hepatic deficiency of ROR α resulted in elevated fasting insulin levels in ROR α^{LKO} mice (Fig. 2g). As elevated fasting insulin level is an indication of insulin resistance, ROR α^{LKO} mice predisposed to severe insulin resistance than ROR α^{ff} mice. Consistent with elevated fasting insulin level, an investigation of insulin signaling pathways confirmed reduction of phosphorylated AKT, indicating that insulin signaling was impaired in HFD-fed ROR α^{LKO} mice (Fig. 2h). As insulin signaling was impaired in the liver, we performed glucose tolerance tests (GTTs) and insulin tolerance tests (ITTs) to determine if glucose homeostasis was impaired in HFD-fed ROR α^{LKO} mice. Glucose intolerance and insulin resistance were observed in HFD-fed ROR α^{LKO} mice, although CD-fed ROR α^{LKO} mice exhibited little or no difference in glucose homeostasis compared with CD-fed ROR α^{ff} mice (Fig. 2i, j). Altogether, our data strongly demonstrate that hepatic ROR α is required for prevention against insulin resistance.

ROR α^{LKO} mice exhibit enhanced PPAR γ transcriptional activity. To explore molecular mechanism by which hepatic deletion of ROR α induces obesity and insulin resistance, we performed mRNA-sequencing analysis of liver tissues obtained from HFD-fed ROR α^{ff} , HFD-fed ROR α^{LKO} , CD-fed ROR α^{ff} and CD-fed ROR α^{LKO} mice (Supplementary Data Table 1). Using the resulting mRNA expression profiles, we first identified 343 differentially expressed genes (DEGs; see Methods) between HFD-fed ROR α^{LKO} and HFD-fed ROR α^{ff} mice (ROR α^{LKO} /ROR α^{ff} _{HFD} in Fig. 3a) and also 395 DEGs between CD-fed ROR α^{LKO} and CD-fed ROR α^{ff} mice (ROR α^{LKO} /ROR α^{ff} _{CD} in Fig. 3a and Supplementary Data 2). Moreover, we further compared log₂-fold changes of the DEGs in the two comparisons above ((ROR α^{LKO} /ROR α^{ff} _{HFD})/(ROR α^{LKO} /ROR α^{ff} _{CD}) in Fig. 3a) and identified the genes specifically affected by ROR α under HFD condition as the DEGs showing significant ($P < 0.05$) differences in the log₂-fold changes (Supplementary Data 2). We categorized these DEGs into eight groups (Groups 1–8) based on differential expression patterns in the three comparisons above. Our data above showed that we only found significant weight gain of ROR α^{LKO} mice under HFD condition. Of Groups 1–8, thus, we first focused on Groups 1–4 showing significant changes under HFD condition (Fig. 3a).

To understand cellular processes represented by Groups 1–4, we performed enrichment analysis of gene ontology biological processes (GOBPs) and Kyoto Encyclopedia of Genes and Genomes (KEGG) pathways for the genes in Groups 1–4 using DAVID software^{33, 34} (Supplementary Data 3). Group 1 is

mainly involved in the processes related to PPAR and adipocytokine signaling pathways and fatty acid/retinol metabolism (Fig. 3b). Group 4 is mainly involved in the processes related to circadian rhythm (Supplementary Data 3). Since Group 1 is highly associated with the weight gain of HFD-fed ROR α^{LKO} , we next examined which transcription factors (TFs) account for up-regulation of the genes in Group 1 under HFD condition. By performing TF enrichment analysis of the genes in Group 1 using ChEA2 software³⁵, PPAR γ turned out to be the most enriched TF in Group 1 (Fig. 3c and Supplementary Data 4). Quantitative PCR with reverse transcription analysis confirmed that the genes in Group 1 including PPAR γ target genes are largely elevated in HFD-fed ROR α^{LKO} mice (Fig. 3d), indicating that PPAR γ transcriptional activity is enhanced in the absence of ROR α .

PPAR α is a transcriptional factor that conducts a key role in hepatic lipid metabolism and shares similar response elements with PPAR γ on the target promoters^{36, 37}. To determine whether ROR α also mediates PPAR α transcriptional network in the liver, we examined the expression of well-known hepatic PPAR α target genes, including *Acox1* and *Fgf21*. The hepatic gene expressions of *Acox1* and *Fgf21* in HFD-fed ROR α^{LKO} mice were similar to those of HFD-fed ROR α^{ff} mice, suggesting that ROR α deficiency would not further enhance hepatic PPAR α transcriptional network (Supplementary Fig. 2a) under HFD condition. We next examined the expression of PPAR α target genes in the physiological setting of PPAR α activation. It has been widely accepted that PPAR α is activated under conditions of energy deprivation³⁸. The induction of PPAR α target genes in ROR α^{LKO} mice was quite similar to that of ROR α^{ff} mice (Supplementary Fig. 2b). Chromatin immunoprecipitation (ChIP) assay clearly revealed little or no difference of PPAR α recruitment to PPAR-response element (PPRE) on the promoters of PPAR α target genes (Supplementary Fig. 2c). Recently, PPAR α has been reported to bind autophagic gene promoters to coordinate autophagy in response to nutrient deprivation³⁷. We observed that the induction of autophagic genes including *LC3a* and *Sesn2* of ROR α^{LKO} mice were similar to those of ROR α^{ff} mice (Supplementary Fig. 2d). Taken together, these data indicate that ROR α mainly controls PPAR γ transcriptional network rather than PPAR α in the liver in response to environmental stress such as HFD.

ROR α represses PPAR γ transcriptional activity via HDAC3. Since PGC1 α is a well-known coactivator for PPAR γ ³⁹, we examined whether introduction of ROR α inhibits PPAR γ /PGC1 α -dependent transcriptional activation using PPRE-containing luciferase reporter. Expression of PGC1 α

Fig. 1 Liver-specific *Rora* deleted mice are susceptible to diet-induced obesity. **a** Schematic representation of the *Rora* gene-targeting strategy, including a map of the ROR α exon 4 and 5 allele (yellow box) and the targeting vector with loxP sites (red arrowhead), FRT sites (blue box), and puromycin selection gene (green box). Bg: BgIII, Rl: EcoRI, Bh: BamHI, Kp: KpnI, Sp: SpeI. **b** Southern blot analysis to screen correctly targeted *Rora* + /puro ES cell clones. For BamHI digestion, the bands representing WT and mutant alleles were 9.0 kb and 6.8 kb, respectively. PCR analyses with genomic DNA extracted from tail of WT, ROR $\alpha^{\text{+/+}}$, Alb; ROR $\alpha^{\text{+/+}}$, ROR α^{ff} and Alb; ROR α^{ff} mice are shown. PCR were performed to amplify the cre (top), floxed and deleted allele (bottom). **c, d** mRNA expression level of ROR α in liver extract **c** and primary hepatocyte **d** from ROR α^{ff} and ROR α^{LKO} mice. Expression was normalized to 18 s rRNA expression. **e, f** Protein expression level of ROR α in liver extract **e** and primary hepatocyte **f**. **g** Body weight change in ROR α^{ff} and ROR α^{LKO} mice fed CD or HFD for 10 weeks ($n = 9$ –12/group). Statistical analysis was performed using Student's unpaired t-test. * $P < 0.05$, ROR α^{ff} vs. ROR α^{LKO} , HFD. **h, i** ROR α^{ff} and ROR α^{LKO} mice were fed with HFD for 10 weeks. **h** Body composition analysis of ROR α^{ff} and ROR α^{LKO} mice ($n = 6$ /group). **i** Macroscopic views of ROR α^{ff} and ROR α^{LKO} mice. **j** Adipose tissues weight of ROR α^{ff} and ROR α^{LKO} mice ($n = 6$ –7/group). **k** Representative image of epididymal white adipose tissue (eWAT) from ROR α^{ff} and ROR α^{LKO} mice stained with hematoxylin and eosin. Scale bar, 100 μm . **l, m** Expression levels of inflammatory cytokine genes in eWAT extract **l** or thermogenesis genes in BAT extract **m** from ROR α^{ff} and ROR α^{LKO} mice ($n = 4$ –5 per group) as determined by qRT-PCR. Expression was normalized to L32 expression. **n** Metabolic cage studies were performed in ROR α^{ff} and ROR α^{LKO} mice ($n = 5$ –6 mice/group). O₂ consumption (VO₂), CO₂ production (VCO₂) and energy expenditure were represented (left to right). Statistical analysis was performed using Student's unpaired t-test. * $P < 0.05$, ** $P < 0.01$, *** $P < 0.001$, NS, Non-Significant. Data expressed as mean \pm s.e.m

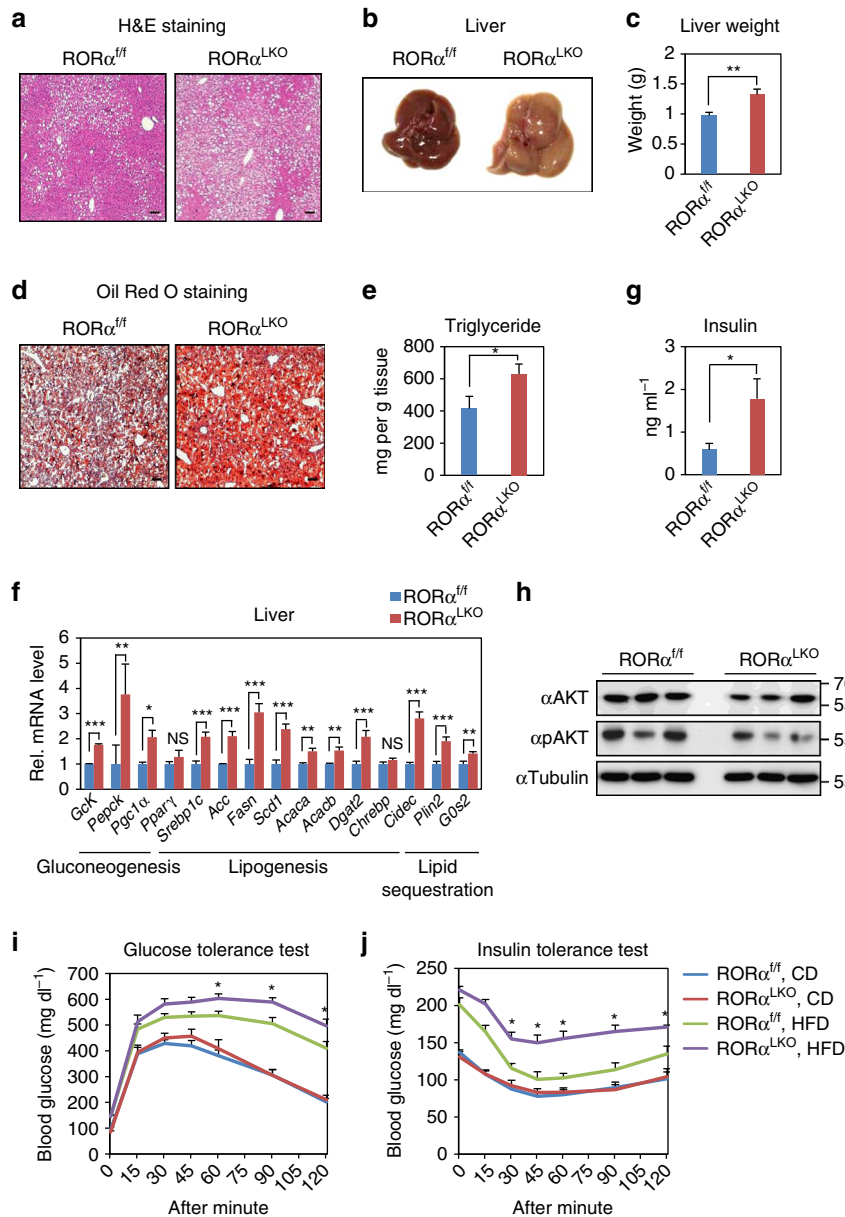


Fig. 2 Liver-specific *Rorα* deleted mice are susceptible to diet-induced hepatic steatosis and insulin resistance. **a–j** ROR $\alpha^{f/f}$ and ROR α^{LKO} mice were fed with HFD for 10 weeks. **a** Representative liver histological section images of ROR $\alpha^{f/f}$ and ROR α^{LKO} mice stained with hematoxylin and eosin. Scale bar, 100 μ m. **b** Macroscopic view of livers from ROR $\alpha^{f/f}$ and ROR α^{LKO} mice. **c** Liver weights of ROR $\alpha^{f/f}$ and ROR α^{LKO} mice ($n = 10–11$ per group). **d** Representative liver histological section images of ROR $\alpha^{f/f}$ and ROR α^{LKO} mice stained with Oil Red O. Scale bar, 100 μ m. **e** Triglyceride content of livers from ROR $\alpha^{f/f}$ and ROR α^{LKO} mice ($n = 8$ per group). **f** Hepatic gene expression profile involved in metabolism from the livers of ROR $\alpha^{f/f}$ and ROR α^{LKO} mice ($n = 4$ per group) as determined by quantitative PCR with reverse transcription (qRT-PCR). Expression was normalized to 36B4 expression. **g** Fasting insulin levels in ROR $\alpha^{f/f}$ and ROR α^{LKO} mice ($n = 6–7$ per group). Data expressed as mean \pm s.e.m. Statistical analysis was performed using Student’s unpaired *t*-test. * $P < 0.05$, ** $P < 0.01$, *** $P < 0.001$, NS = non-significant. **h** Immunoblot analysis was performed from liver extracts of ROR $\alpha^{f/f}$ and ROR α^{LKO} mice. **i, j** Glucose tolerance test **i** and insulin tolerance test **j** on ROR $\alpha^{f/f}$ and ROR α^{LKO} mice fed on CD or HFD for 10 weeks. ($n = 4–9$ /group). Data expressed as mean \pm s.e.m. Statistical analysis was performed using Student’s unpaired *t*-test. * $P < 0.05$, ROR $\alpha^{f/f}$ vs ROR α^{LKO} , HFD. Data expressed as mean \pm s.e.m.

dramatically increased PPAR γ transcriptional activity, and increased expression of ROR α progressively attenuated the PPAR γ /PGC1 α -dependent transcriptional activation (Fig. 4a). In addition, we examined whether ROR α inhibits NCOA1 and NCOA2-mediated PPAR γ transcriptional activation. NCOA1 and NCOA2, as p160 family members, are also coactivators for PPAR γ ⁴⁰. Consistently, ROR α significantly reduced NCOA1 and NCOA2-mediated transcriptional activation (Fig. 4b and Supplementary Fig. 3a).

To evaluate the role of ROR α in attenuation of the PPAR γ -dependent transcriptional activation, we treated Hep3B cells with rosiglitazone, a PPAR γ synthetic agonist, and then measured PPRE-luciferase activity. Knockdown of ROR α markedly enhanced PPRE-luciferase activity, indicating that ROR α functions to repress PPAR γ transcriptional activity (Fig. 4c). To determine if DNA-binding domain (DBD) of ROR α is required for inhibiting PPAR γ transcriptional activation, we introduced DBD-deleted ROR α mutant (ROR α Δ DBD). We observed

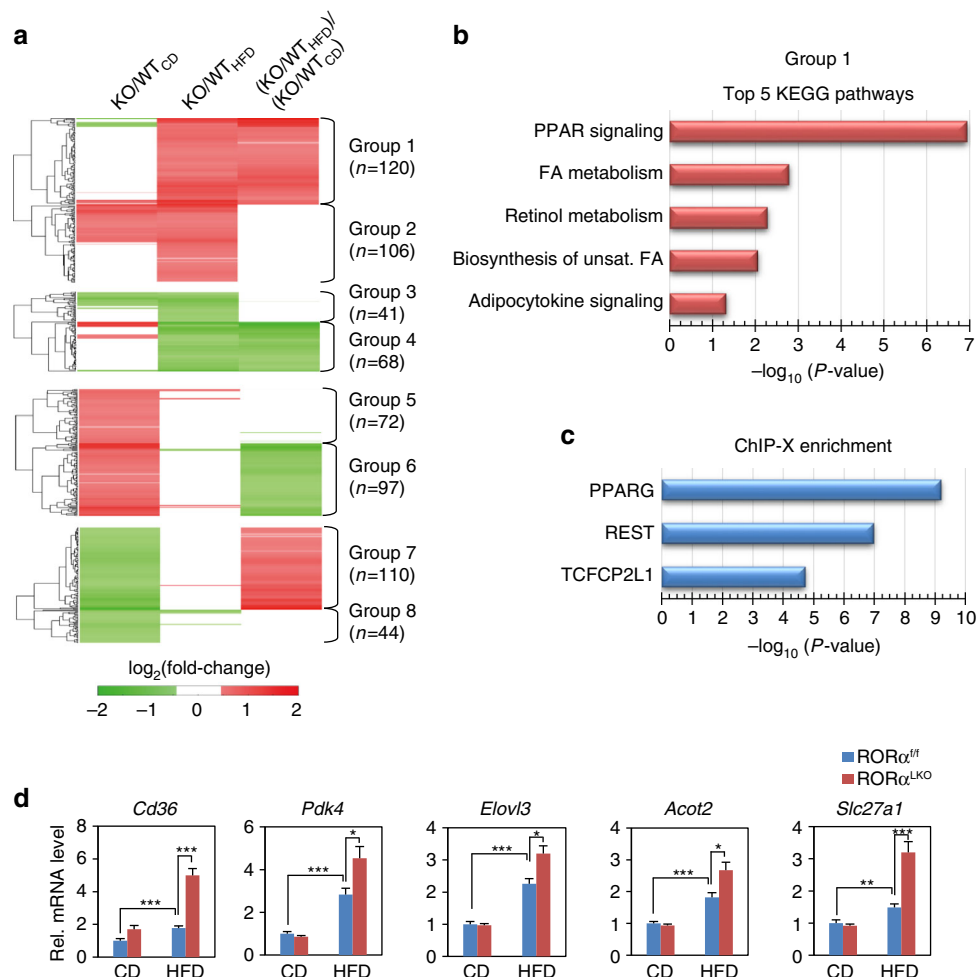


Fig. 3 Transcriptome analysis of hepatic gene expression profile in $ROR\alpha^{LKO}$ mice. **a** Up- and down-regulated genes in $ROR\alpha^{LKO}$ compared to $ROR\alpha^{f/f}$ mice. These genes were categorized into four groups of the up- (Groups 1, 2) and down-regulated genes (Groups 3, 4) in HFD-fed $ROR\alpha^{LKO}$. Besides Groups 1–4, remain genes were also categorized into four groups of the up- (Groups 5, 6) and down-regulated genes (Groups 7, 8) in CD-fed $ROR\alpha^{LKO}$. Groups 1, 2 (or Groups 3, 4) were further divided by the specificity of the $ROR\alpha$ effect under HFD condition. \log_2 -fold changes in the following comparisons were displayed: $ROR\alpha^{LKO}/ROR\alpha^{f/f}_{HFD}$, $ROR\alpha^{LKO}/ROR\alpha^{f/f}_{CD}$ and $(ROR\alpha^{LKO}/ROR\alpha^{f/f}_{HFD})/(ROR\alpha^{LKO}/ROR\alpha^{f/f}_{CD})$. Hierarchical clustering of the DEGs in Groups 1–8 (Euclidian distance as a dissimilarity measure and average linkage) were used to display the \log_2 -fold changes. **b** KEGG pathways enrichment analysis for the genes in Group 1. The bars represent the enrichment scores, $-\log_{10}(P\text{ value})$. **c** TF enrichment analysis for the genes in Group 1 using ChEA2 software. Top 3 TFs are shown. The bars represent the enrichment scores, $-\log_{10}(P\text{ value})$. **d** Expression levels of group 1 genes (upregulated genes in $ROR\alpha^{LKO}$ mice fed HFD compared with $ROR\alpha^{f/f}$ mice) in liver extract from $ROR\alpha^{f/f}$ and $ROR\alpha^{LKO}$ mice fed CD or HFD for 10 weeks ($n=5$ –9/group) as determined by qRT-PCR. Expression was normalized to 36B4 expression. Statistical analysis was performed using two-way ANOVA. * $P < 0.05$, ** $P < 0.01$, *** $P < 0.001$. Data expressed as mean \pm s.e.m

that $ROR\alpha$ WT markedly suppressed $PPAR\gamma$ transcriptional activation, whereas the $ROR\alpha$ -mediated repression was remarkably relieved by introduction of $ROR\alpha \Delta DBD$ (Fig. 4d). As $ROR\alpha$ failed to interact with $PPAR\gamma$, our data proposed that $ROR\alpha$ suppresses $PPAR\gamma$ transcriptional activation through DBD and possibly competes with $PPAR\gamma$ for the binding to PPRE. Consistently, the recruitment of $ROR\alpha$ was markedly reduced in PPRE-deleted synthetic promoter region (Supplementary Fig. 3b, c).

Since histone acetylation promotes transcriptional activation, we next examined whether $ROR\alpha$ interacts with specific histone deacetylases for the repression of $PPAR\gamma$ transcriptional activity. Co-immunoprecipitation assay revealed that $ROR\alpha$ specifically interacts with HDAC3 (Fig. 4e and Supplementary Fig. 3d). To determine if HDAC3 is required for $ROR\alpha$ -mediated repression of $PPAR\gamma$ transcriptional activity, we further examined repressive function of HDAC3 for PPRE-luciferase activity in the presence or absence of $ROR\alpha$. Intriguingly, knockdown of $ROR\alpha$ relieved

the HDAC3-dependent repressive function indicating that HDAC3 exerted repressive function on $PPAR\gamma$ transcriptional activity in the presence of $ROR\alpha$ (Fig. 4f). Consistently, knockdown of HDAC3 largely reversed $ROR\alpha$ -mediated repression of $PPAR\gamma$ transcriptional activity (Fig. 4g, h and Supplementary Fig. 3e). These results indicate that $ROR\alpha$ recruits HDAC3 to potentiate repression of $PPAR\gamma$ transcriptional activity.

$ROR\alpha$ /HDAC3 dynamically regulate $PPAR\gamma$ target gene expression. PPRE consists of a direct repeat (DR) sequence of (A/G)GGTCA spaced by one nucleotide, whereas consensus $ROR\alpha$ response element (RORE) consists of core motif (A/G)GGTCA preceded by a 6-bp A/T-rich sequence. Thus, given that RORE and PPRE share core motif, we hypothesized that $ROR\alpha$ directly binds the PPRE of $PPAR\gamma$ target promoters for transcriptional repression. To examine whether $ROR\alpha$ and

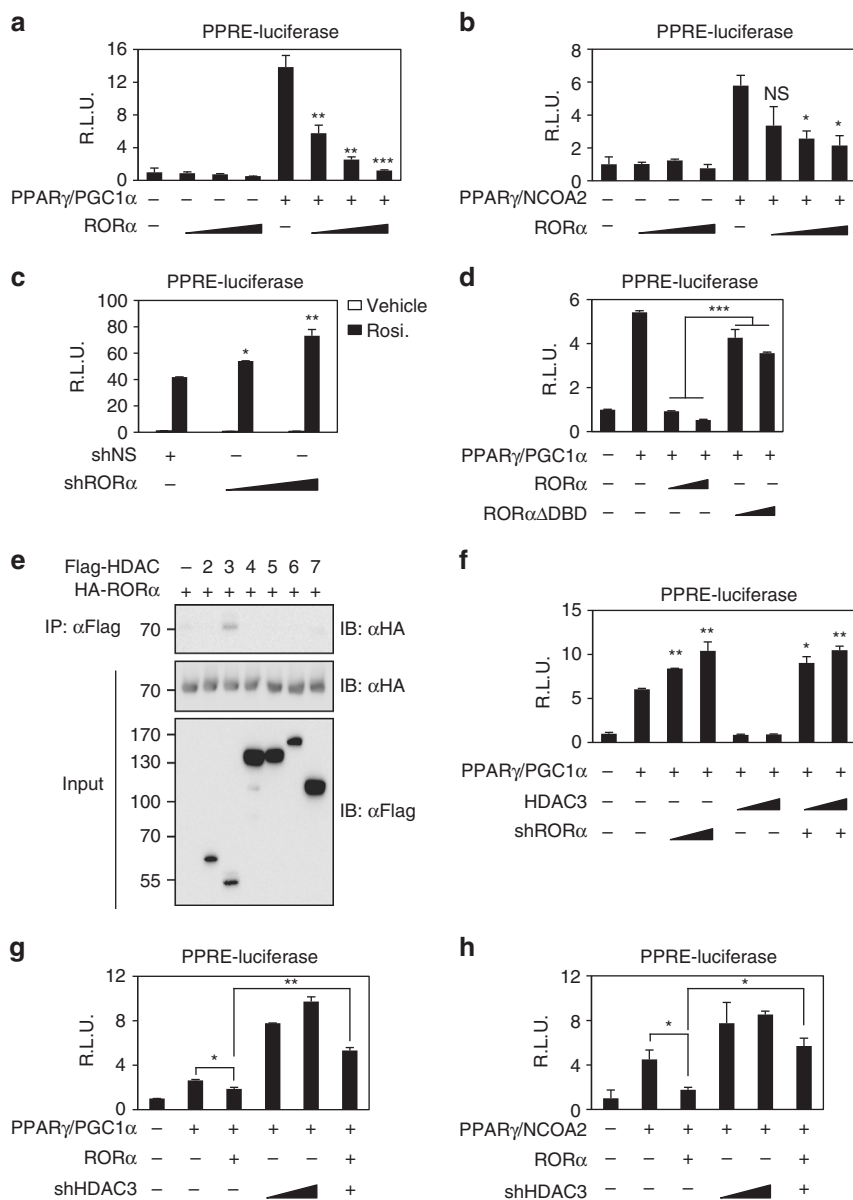


Fig. 4 ROR α interacts with HDAC3 to repress PPAR γ transcriptional activity. **a**, **b** Effect of overexpression of ROR α on PPRE-luciferase reporter activity with coactivator PGC1 α **a** or NCOA2 **b**. * P < 0.05, ** P < 0.01, *** P < 0.001, NS, non-significant, compared to PPAR γ /coactivator group. **c** Effect of knockdown of ROR α on PPRE-luciferase reporter activity. Cells were treated with DMSO (vehicle), rosiglitazone (20 μ M) for 24 h. * P < 0.05, ** P < 0.01, compared to shNS group. **d** Effect of ROR α Δ DBD mutant on PPRE-luciferase reporter activity. *** P < 0.001. **e** Co-immunoprecipitation assay was performed to detect the interaction between ROR α and HDACs of HEK293T cells. **f** Effect of ROR α on PPRE-luciferase reporter activity by HDAC3 overexpression. * P < 0.05, ** P < 0.01, compared to PPAR γ /PGC1 α group. **g**, **h** Effect of knockdown of HDAC3 with coactivator PGC1 α **g** and NCOA2 **h** on PPRE-luciferase reporter activity. Data expressed as mean \pm s.e.m. Statistical analysis was performed using one-way ANOVA followed by Tukey's post hoc analysis. * P < 0.05, ** P < 0.01. Data expressed as mean \pm s.e.m

HDAC3 are co-recruited to the PPAR γ target promoters for the repression, we performed ChIP assay with anti-ROR α , PPAR γ , PPAR α , RNA polymerase II (Pol II), acetylated H3 (H3Ac) and HDAC3 antibodies from the mouse liver extracts of CD or HFD-fed ROR $\alpha^{fl/fl}$ and ROR α^{LKO} mice. ChIP assays revealed that ROR α and HDAC3 were co-recruited to the *Cd36*, *Scd1* and *Plin2* promoters in the liver of HFD-fed ROR $\alpha^{fl/fl}$ mice, although no changes were observed with CD-fed ROR $\alpha^{fl/fl}$ mice (Fig. 5a and Supplementary Fig. 4a, b). In the absence of ROR α , PPAR γ recruitment was markedly increased, whereas HDAC3 recruitment was largely diminished along with elevated acetylated H3 levels on the *Cd36*, *Scd1* and *Plin2* promoters in the liver of HFD-fed ROR α^{LKO} mice (Fig. 5a and Supplementary Fig. 4a, b). Unlike

PPAR γ , PPAR α recruitment was barely detected from the PPAR γ target promoters containing PPRE as assessed by ChIP assay (Fig. 5a and Supplementary Fig. 4b, c).

We next determined if both ROR α and HDAC3 are recruited to the PPRE in response to PPAR γ agonist in Hep3B cells (Supplementary Fig. 5a). Treatment of rosiglitazone largely induced the expression of PPAR γ target genes (Supplementary Fig. 5b). Interestingly, 8 h washout after rosiglitazone treatment dramatically reduced PPAR γ target gene expressions (Supplementary Fig. 5a, b). Consistent with gene expressions, treatment of rosiglitazone increased recruitment of PPAR γ , PGC1 α and Pol II with elevated histone H3 acetylation level on PPAR γ target promoters as well as induction of PPAR γ target

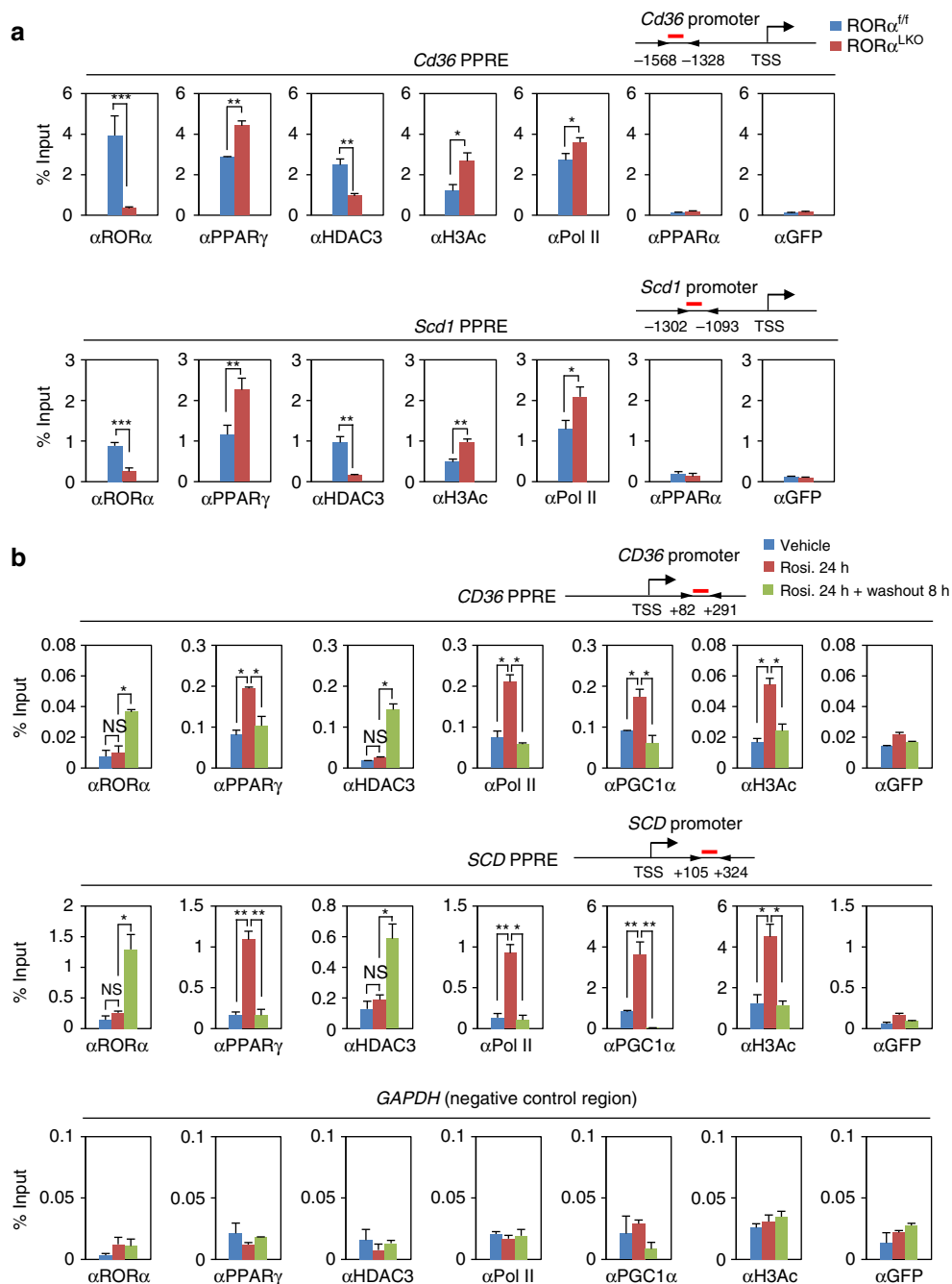


Fig. 5 ROR α recruits to the PPAR γ target gene promoters with HDAC3. **a** ChIP assays were performed on the *Cd36* and *Scd1* promoters in liver extract from ROR $\alpha^{f/f}$ and ROR α^{LKO} mice fed HFD for 10 weeks ($n=3$ per group). Promoter occupancy by ROR α , PPAR γ , HDAC3, H3Ac, Pol II, PPAR α and GFP was analyzed. Schematic of promoter region was represented with gene name. Red bar depicts locations of PPRE. Statistical analysis was performed using Student's unpaired *t*-test. * $P < 0.05$, ** $P < 0.01$, *** $P < 0.001$. **b** ChIP assays were performed on the *CD36*, *SCD* promoters and *GAPDH*-negative region in Hep3B cells with or without Rosiglitazone (20 μ M) treatment for 24 h and washout 8 h. Promoter occupancy of ROR α , PPAR γ , HDAC3, Pol II, PGC1 α , H3Ac and GFP was analyzed. Schematic of promoter region was represented with gene name. Red bar depicts locations of PPRE. Statistical analysis was performed using one-way ANOVA followed by Tukey's post hoc analysis. * $P < 0.05$, ** $P < 0.01$. Data expressed as mean \pm s.e.m

genes (Fig. 5b and Supplementary Fig. 5c). Strikingly, further increased recruitment of ROR α to PPRE was observed along with enhanced HDAC3 recruitment in the setting of washout of rosiglitazone for 8 h (Fig. 5b and Supplementary Fig. 5c). Increased recruitment of ROR α and HDAC3 substantially diminished PGC1 α and Pol II recruitment on PPRE with decreased histone H3 acetylation level on PPRE (Fig. 5b and Supplementary Fig. 5c).

Next, we further determined whether PPAR γ antagonist GW9662 also resulted in the increased recruitment of ROR α and HDAC3 to the PPAR γ target promoters. Consistent with the results from 8 h washout, GW9662 treatment significantly reduced the expression levels of PPAR γ target genes (Supplementary Fig. 6a). ChIP assay revealed that recruitment of ROR α and HDAC3 to the PPAR γ target promoters were markedly increased, while PPAR γ and Pol II recruitments were markedly

reduced in response to GW9662 treatment (Supplementary Fig. 6b).

ROR α competes with PPAR γ for binding to PPAR γ target promoters. To address HDAC3 recruitment to PPAR γ target gene promoters requires ROR α , we first examined the PPAR γ target gene induction in the presence or absence of ROR α . The induction of PPAR γ target genes by rosiglitazone was further enhanced by ROR α siRNA, indicating that ROR α is a critical transcriptional repressor for PPAR γ target gene expression (Supplementary Fig. 7a). ROR α knockdown largely increased the recruitment of PPAR γ for transcriptional activation with increased levels of H3 acetylation to the PPAR γ target gene promoters (Fig. 6a and Supplementary Fig. 7b). While remarkably increased by rosiglitazone washout, the HDAC3 recruitment was substantially reduced by ROR α knockdown even with setting of rosiglitazone washout (Fig. 6a and Supplementary Fig. 7b). Taken together, these data clearly indicate that ROR α is required for recruitment of HDAC3 to PPAR γ target gene promoters.

To determine if ROR α competes with PPAR γ for the binding to the PPAR γ target promoters, we transiently knocked down PPAR γ in Hep3B cells. To mimic HFD feeding conditions in vitro, we treated cells with free fatty acid (FFA) and examined expression of PPAR γ target genes. We observed that FFA treatment markedly increased PPAR γ target gene expressions in both WT and *Ppara*-null mouse primary hepatocytes, indicating that PPAR α failed to influence on PPAR γ transcriptional network in the setting of HFD (Supplementary Fig. 7c). Next, we tested PPAR γ target gene expressions in the presence of PPAR γ siRNA or HDAC3 siRNA. While repressed by PPAR γ siRNA, expression of PPAR γ target genes was largely enhanced by HDAC3 siRNA in response to FFA treatment (Supplementary Fig. 7d). Consistent with gene expression, increased PPAR γ recruitment by FFA was substantially diminished by PPAR γ siRNA (Fig. 6b). Interestingly, recruitment of ROR α was dramatically increased to the PPAR γ target gene promoters, and HDAC3 recruitment was accompanied by the ROR α recruitment to PPAR γ target promoters by knockdown of PPAR γ (Fig. 6b). Furthermore, Re-ChIP assay clearly indicated that PPAR γ and ROR α are able to bind to the same genomic region and their recruitments to promoter of target genes are mutually exclusive (Supplementary Fig. 7e). These data strongly indicate that ROR α and HDAC3 compete with PPAR γ for the binding to the target gene promoters for regulation of gene expressions with opposite transcriptional outputs. Altogether, our data demonstrate that ROR α functions as a corepressor along with HDAC3 and is co-recruited to the PPAR γ target promoters for the repression of PPAR γ -mediated transcriptional activity.

To determine whether ROR α recruitment is accompanied by the presence of HDAC3, we examined recruitment of ROR α to the PPAR γ target gene promoters in the presence of HDAC3 siRNA. Although little or no difference of the recruitment of ROR α and PPAR γ was observed, Pol II recruitment to the PPAR γ target gene promoters was markedly increased by HDAC3 knockdown (Fig. 6c), indicating that the presence of HDAC3 affected the recruitment of RNA polymerase II to the PPAR γ target gene promoters. Taken together, these data indicate that both ROR α and HDAC3 serve as transcriptional corepressors on the PPAR γ target gene promoters for the repression of PPAR γ target gene expressions.

PPAR γ antagonism restores metabolic homeostasis in ROR α ^{LKO} mice. Since ROR α turned out to play a key role to repress PPAR γ transcriptional activity in vitro and in vivo, we next examined if inhibition of PPAR γ transcriptional activities restores impaired metabolic homeostasis. For this, PPAR γ

antagonist GW9662 were treated to ROR α ^{ff} and ROR α ^{LKO} mice for 5 weeks with HFD. Intriguingly, the body weight gain of both ROR α ^{ff} and ROR α ^{LKO} mice were markedly reduced by GW9662 treatment compared with vehicle-treated control mice (Fig. 7a). The reduction of body weight gain by GW9662 in ROR α ^{LKO} mice was much greater, leading to similar body weight to GW9662-treated ROR α ^{ff} mice, indicating that inhibition of PPAR γ activity remarkably reduces body weight gain in ROR α ^{LKO} mice (Fig. 7a). Similar to reduced body weight gain, tissue weights of the liver and epididymal white adipose tissue were markedly reduced by GW9662 treatment in both ROR α ^{ff} and ROR α ^{LKO} mice (Fig. 7b, c). Consistently, cross-sectional area of adipocytes was significantly reduced by GW9662 treatment (Fig. 7d). In accordance with body weight reduction, PPAR γ antagonism markedly reduced hepatic steatosis in both ROR α ^{ff} and ROR α ^{LKO} mice (Fig. 7e). Consistently, gene expression profile analysis exhibited that target gene expression levels involved in hepatic gluconeogenesis and lipogenesis are largely reduced by GW9662 treatment (Fig. 7f, g). Together, we demonstrate that enhanced PPAR γ transcriptional activity by ROR α deficiency is de-activated by PPAR γ antagonism to restore metabolic homeostasis, including body weight gain, hepatic steatosis and glucose and lipid metabolism.

Discussion

Hepatic nuclear receptors play critical roles in the regulation of lipid and glucose metabolism in response to environmental stress, including nutrient and hormonal cues⁴¹. Dysfunction of hepatic nuclear receptors is largely linked to metabolic diseases including obesity and type II diabetes. We found that PPAR γ signaling is a critical pathway affected by hepatic deletion of ROR α . Dysregulated PPAR γ signaling in ROR α ^{LKO} mice results in uncontrolled lipogenesis, contributing to the development of hepatic steatosis and diet-induced obesity on a HFD. Furthermore, treatment of PPAR γ antagonist GW9662 decreased the susceptibility to obesity^{42, 43}. Consistent with previous reports, we also observed that elevated PPAR γ transcriptional activity in ROR α ^{LKO} mice are downregulated after treatment of GW9662, resulting in decrease of diet-induced hepatic steatosis and obesity. Our data confirm that ROR α is a key factor for the repression of PPAR γ signaling to protect against diet-induced hepatic steatosis and obesity in vivo.

Together, PPAR γ signaling turns out to be significantly activated in HFD-fed ROR α ^{LKO} mice while increased ROR α reduces PPAR γ transcriptional activity, providing a direct molecular link between ROR α and PPAR γ . Furthermore, our data indicate that ROR α regulates PPAR γ signaling through ROR α -mediated HDAC3 recruitment to the PPAR γ target promoters. Thus, ROR α plays a crucial role in maintaining homeostasis of lipid metabolism in liver by negatively regulating PPAR γ signaling via HDAC3 recruitment to the PPAR γ target promoters for transcriptional repression (Fig. 7h).

Thiazolidinedione (TZD) is a synthetic PPAR γ agonist and has been clinically approved to improve glucose homeostasis and fatty liver in human patients. Although the molecular mechanisms still remain unclear, the 'lipid steal' hypothesis has been widely accepted to explain of how TZD treatment improves insulin resistance in type II diabetes patients^{44–46}. However, though PPAR γ activation has shown to reduce blood glucose level and hepatic gluconeogenesis, and improve glucose tolerance^{47, 48}, several reports have shown that PPAR γ activation leads to hepatic steatosis^{49, 50}. In general, the expression of PPAR γ is very low in human and mouse liver. Interestingly, the expression level of hepatic PPAR γ is significantly upregulated in obese rodent model⁵¹ and high level of PPAR γ in mouse liver is sufficient for

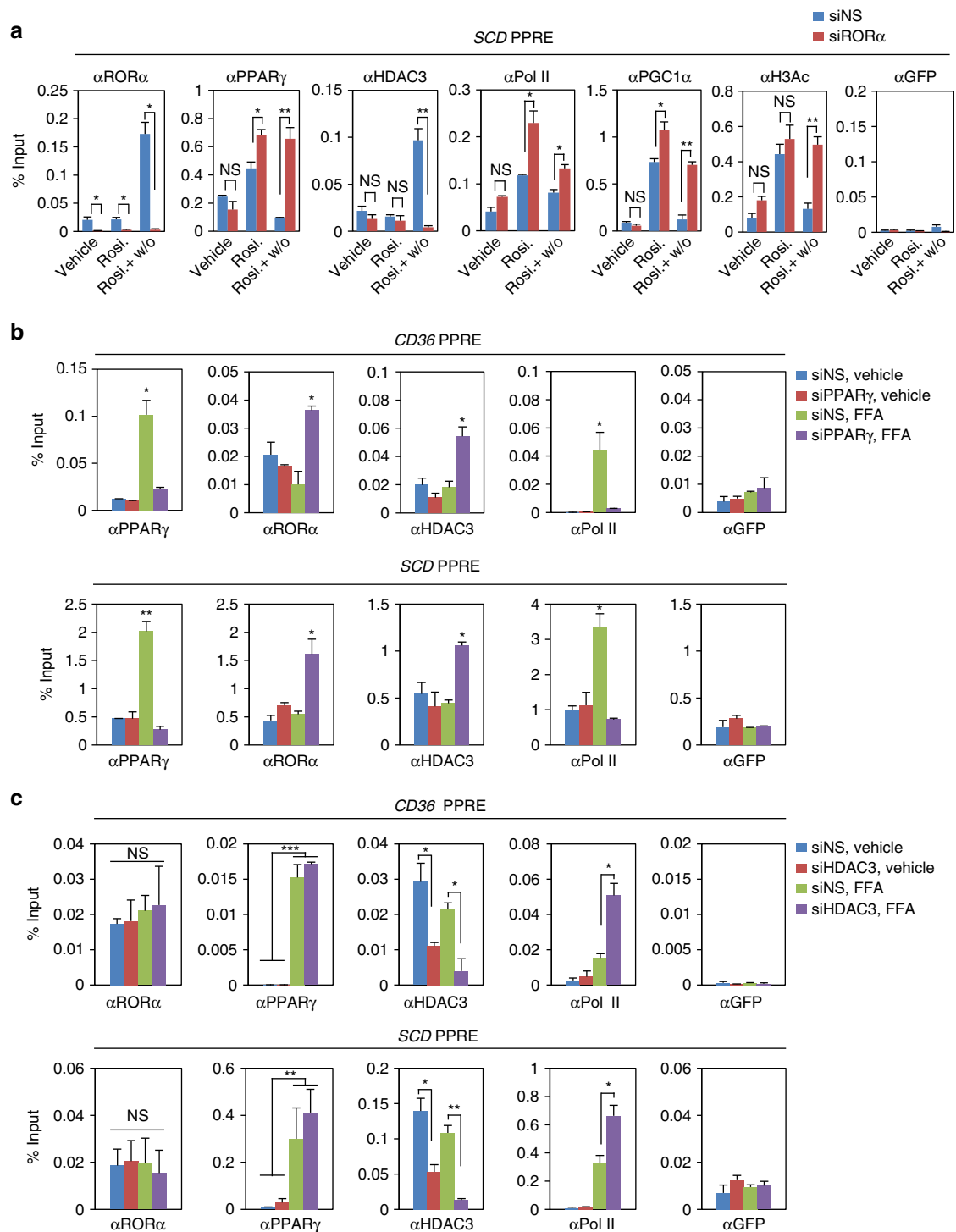


Fig. 6 Recruitment of ROR α and PPAR γ to the PPAR γ target gene promoters are mutually exclusive. **a** ChIP assays were performed in the absence or presence of ROR α on SCD promoters in Hep3B cells with or without Rosiglitazone (20 μ M) treatment for 24 h and washout 8 h. Promoter occupancy of ROR α , PPAR γ , HDAC3, Pol II, PGC1 α , H3Ac and GFP was analyzed. Statistical analysis was performed using Student's unpaired *t*-test. **P* < 0.05, ***P* < 0.01, NS, non-significant. **b, c** ChIP assays were performed in the absence or presence of PPAR γ b/HDAC3 c on the CD36 and SCD promoters in Hep3B cells with or without free fatty acid (free fatty acid: Oleic acid 200 μ M and Palmitic acid 100 μ M) treatment for 24 h. Promoter occupancy of PPAR γ , ROR α , HDAC3, Pol II and GFP was analyzed. Data expressed as mean \pm s.e.m. Statistical analysis was performed using one-way ANOVA. **P* < 0.05, ***P* < 0.01, ****P* < 0.001. Data expressed as mean \pm s.e.m

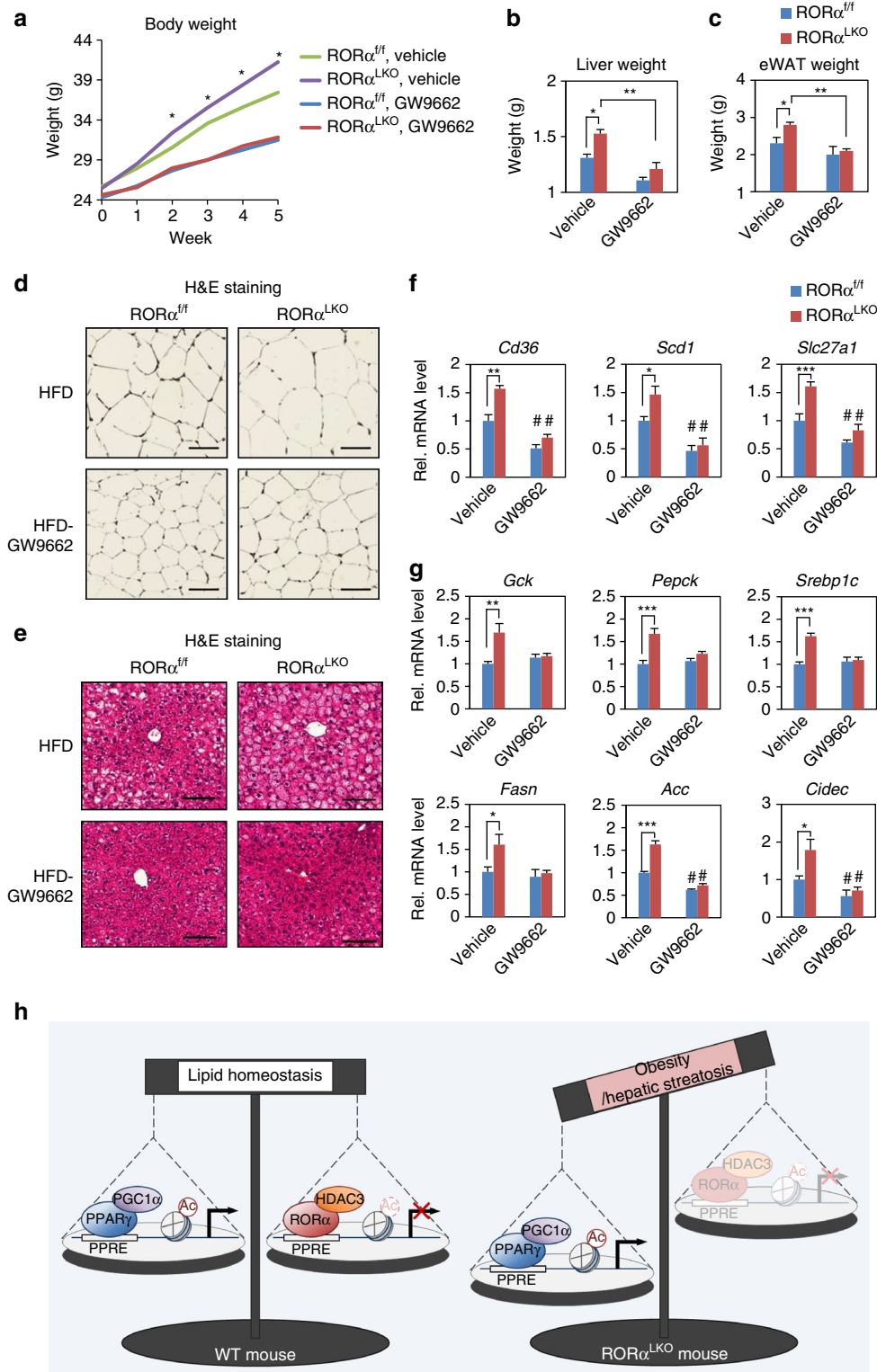
the induction of adipogenic transformation of hepatocytes with adipose tissue-specific gene expression and lipid accumulation⁵². These data indicate that PPAR γ plays a key role in development of hepatic steatosis. Accordingly, inhibition of PPAR γ signaling and hepatic deficiency of PPAR γ in ob/ob mice have shown to

ameliorate fatty liver^{53, 54}. A recent study clearly showed that PPAR γ antagonism improves insulin sensitivity, promotes the browning of white adipose tissue and reduces lipogenic and glucogenic gene expressions in the liver to prevent against diet-induced obesity⁵⁵. Intriguingly, liver-specific PPAR γ -

deficient mice exhibit resistance to HFD-induced hepatic steatosis⁵⁶. Expression of numerous genes involved in lipid uptake and lipid transport was remarkably decreased in the liver-specific PPAR γ -deficient mice, resulting in reduction of hepatic steatosis⁵⁶. Altogether, these studies suggest that local activation of hepatic PPAR γ may promote ectopic fat deposition in the liver whereas systemic activation of PPAR γ may promote fat deposition in adipose tissue rather than liver leading to clinical improvements of metabolic syndromes including hepatic

steatosis. Thus, negative control of ROR α to suppress hepatic PPAR γ activation is important to maintain physiological hepatic lipid homeostasis. Therefore, these results strongly indicate that the PPAR γ signaling pathway is involved in diet-induced hepatic steatosis, and hepatic lipid accumulation is prevented by suppression of PPAR γ transcriptional network in the liver.

It has been widely accepted that PPAR α is a major nutrient-sensing PPAR isoform to modulate hepatic gene expressions³⁷. As no substantial activation of PPAR α has been



observed in the fasted or HFD-fed $ROR\alpha^{LKO}$ mice, we believe that $ROR\alpha$ mainly controls $PPAR\gamma$ transcriptional network to maintain hepatic homeostasis in response to HFD. However, it has been well established that $PPAR\alpha$ is a promising therapeutic target to upregulate beta oxidation gene expressions and inhibit hepatic de novo lipogenesis. Consistently, animal model using $PPAR\alpha$ -null mice have been reported to develop remarkable hepatic steatosis^{38, 57}. Thus, it is highly possible that hepatic steatosis phenotype in HFD-fed $ROR\alpha^{LKO}$ mice may be resulted from both upregulated $PPAR\gamma$ activation and suppressed $PPAR\alpha$ transcriptional activity in the absence of $ROR\alpha$. Understanding of the contribution of $PPAR\alpha$ transcriptional network with $ROR\alpha$ would be critical to delineate the molecular mechanisms of how $PPAR$ isoforms including $PPAR\alpha$ and $PPAR\gamma$ modulate hepatic lipid homeostasis with various transcriptional factors in response to environmental stress such as HFD.

It has been reported that $ROR\alpha$ may compete with $PPAR\gamma$ for the binding to PPRES⁵⁸. It is well established that PPRES contains a DR1 motif consisting of two core DRs of AGGTCA separated by a single nucleotide⁵⁹. Among nucleotides of DR1 motif, the four nucleotides immediately 5' of DR1 motif are highly conserved and exhibit a consensus of A(A/T)CT. Previous study has reported that the binding of the DBD of $PPARs$ to the single core binding site requires the AT-rich 5'-extended binding site which is quite similar to the binding site for the monomer of $ROR\alpha$ ⁶⁰. Thus, the similarity in the binding sequences for $PPAR\gamma$ and $ROR\alpha$ appears to allow $ROR\alpha$ to modulate $PPAR$ signaling by competing with $PPAR\gamma$ for binding to PPRES⁶¹.

The physiological role of HDAC3 has been reported to repress hepatic steatosis. In liver-specific *Hdac3*-deficient mice, little or no body weight change was observed. As HDAC3 regulates the expression of lipogenic genes in an enzymatic activity-independent manner⁶², fasting phase markedly promotes hepatic steatosis in liver-specific *Hdac3*-deficient mice⁶³. An intriguing observation in this study is that $ROR\alpha$ is crucial to recruit HDAC3 to repress hepatic $PPAR\gamma$ -mediated lipogenic genes and protect against diet-induced hepatic steatosis and obesity. Furthermore, repressive role of $ROR\alpha$ -mediated HDAC3 on lipid metabolism is coupled with elevated hepatic gluconeogenesis. Though hepatic HDAC3 has been shown to promote gluconeogenesis by repressing lipid synthesis and sequestration⁶³, we observed notable increase of gene expression involved in hepatic gluconeogenesis in HFD-fed $ROR\alpha^{LKO}$ mice. Intriguingly, HDAC3 ablation upregulated hepatic expression of perilipin gene which contributes to lipid sequestration to ameliorate glucose tolerance⁶³. We also noticed that perilipin 2, hepatic isoform of perilipin was substantially elevated in HFD-fed $ROR\alpha^{LKO}$ mice. Unlike hepatic HDAC3 ablation, impaired $ROR\alpha$ -mediated HDAC3 transcriptional repression led to interfere hepatic homeostasis of $PPAR\gamma$ signaling. Therefore, disturbed regulatory mechanism of $PPAR\gamma$ signaling in HFD-fed $ROR\alpha^{LKO}$ mice would be the main cause of the insulin resistance

and glucose intolerance. Consistent with elevated fasting glucose level in HFD-fed $ROR\alpha^{LKO}$ mice, mRNA level of the rate-limiting enzyme, phosphoenol pyruvate carboxykinase (PEPCK), in the hepatic gluconeogenesis pathway, was largely elevated in HFD-fed $ROR\alpha^{LKO}$ mice. Together, our data strongly indicate that physiological role of HDAC3 in the liver is to suppress $PPAR\gamma$ transcriptional activity via $ROR\alpha$ to control hepatic lipid and glucose metabolism.

Previously, it has been reported that bile acid signaling pathway is critical to modulate EE in brown adipose tissue. Bile acids activates mitogen-activated protein kinase pathways and serve as ligands for the G protein-coupled receptor TGR5²⁹. Thus, hepatic bile acid synthesis and bile acid pool size in the serum is critical to control metabolic rate. Bile acids induces cyclic-AMP-dependent thyroid hormone activating enzyme type 2 iodothyronine deiodinase (D2)²⁹. Thus, bile acid-TGR5-cAMP-D2 signaling pathway in the brown adipose tissue has been known as a crucial mechanism to modulate EE²⁹. We observed that several key genes involved in bile acid synthesis were largely downregulated as well as serum bile acid pool size in HFD-fed $ROR\alpha^{LKO}$ mice. Though we still do not know the direct mechanism of how hepatic bile acid signaling was impaired in $ROR\alpha^{LKO}$ mice, we speculate that impaired hepatic bile acid synthesis would impair TGR5 activation in brown adipose tissue to reduce EE.

Several of the observed metabolic alterations in the $ROR\alpha^{LKO}$ mice are indeed different from those observed in *sg* mice. For example, $ROR\alpha^{LKO}$ mice gain significantly more weight than WT mice and develop hepatic steatosis when fed with HFD. However, *sg* mice are protected from HFD-induced obesity and fatty liver and display improved insulin sensitivity^{28, 64}. A strong difference between these two mouse models is their overall growth condition. $ROR\alpha^{LKO}$ mice have no obvious phenotypic abnormalities under normal dietary conditions, whereas *sg* mice suffer from severe growth retardation that would likely be attributed to a number of developmental defects. In addition, defective $ROR\alpha$ function in other tissues including brain is likely to systemically affect energy intake and expenditure in the *sg* mice, making it difficult to specifically dissect hepatic function of $ROR\alpha$. Therefore, it would be helpful to utilize these two mice and compare their phenotypes in certain conditions together for understanding of $ROR\alpha$ function *in vivo*. Collectively, our data indicate that liver-specific $ROR\alpha$ deficient mice were successfully developed and the utilization of the mice allowed us to be able to study *in vivo* functions of $ROR\alpha$ in liver more precisely by excluding the potential secondary effect of *sg* mice.

In conclusion, our data indicate that $ROR\alpha$ requires HDAC3 to regulate $PPAR\gamma$ signaling to maintain lipid homeostasis in response to over-nutrient cue. We demonstrate that major target of $ROR\alpha$ in the liver is the $PPAR\gamma$ signaling and lipid/glucose metabolism. Our findings provide a direct link between $ROR\alpha$ and hepatic fatty acid and glucose metabolism. Thus, therapeutic

Fig. 7 $PPAR\gamma$ antagonism restores metabolic homeostasis in $ROR\alpha^{LKO}$ mice. **a–e** $ROR\alpha^{f/f}$ and $ROR\alpha^{LKO}$ mice were fed HFD with or without GW9662 for 5 weeks ($n = 4–5$ per group). **a** Body weight curves. Statistical analysis was performed using Student's unpaired *t*-test. * $P < 0.05$, $ROR\alpha^{f/f}$ vs $ROR\alpha^{LKO}$, vehicle. **b, c** Liver **b** and epididymal white adipose tissue (eWAT) **c** weight of $ROR\alpha^{f/f}$ and $ROR\alpha^{LKO}$ mice were fed HFD with or without GW9662 for 5 weeks. Statistical analysis was performed using two-way ANOVA. * $P < 0.05$, ** $P < 0.01$. **d, e** Representative histological section images from eWAT **d** and liver **e** of $ROR\alpha^{f/f}$ and $ROR\alpha^{LKO}$ mice fed HFD with or without GW9662 for 5 weeks. Scale bar, 100 μm . **f, g** Expression levels of $PPAR\gamma$ target genes **f** or gluconeogenesis/lipogenesis/lipid sequestration genes **g** in liver from $ROR\alpha^{f/f}$ and $ROR\alpha^{LKO}$ mice fed HFD with or without GW9662 for 5 weeks as determined by quantitative PCR with reverse transcription. Expression was normalized to 36B4 expression. Statistical analysis was performed using Student's unpaired *t*-test. * $P < 0.05$, ** $P < 0.01$, *** $P < 0.001$, # $P < 0.05$ compared to each vehicle group. Data expressed as mean \pm s.e.m. **h** Proposed model for the role of $ROR\alpha$ in hepatocyte. $ROR\alpha$ regulates $PPAR\gamma$ signaling via HDAC3 recruitment to the $PPAR\gamma$ target promoters for transcriptional repression

strategies designed to modulate ROR α activity may be beneficial for the treatment of hepatic disease as well as obesity-associated metabolic diseases.

Methods

Generation of conditional Ror α -deficient mice and animal care. To generate mice with a floxed ROR α allele, a 16.5 kb region used to construct the targeting vector was first subcloned from a BAC clone (bMQ-293I20, Source BioScience) into a pBluescript phagemid system. The FRT-flanked puromycin cassette containing a loxP sequence was inserted at the front of exon 4 and the single loxP site was inserted at the back of exon 5. The target region was ~15.2 kb which included exons 4 and 5. Twenty micrograms of the targeting vector was linearized by SalI and then electroporated to E14Tg2A ES cells. Surviving clones after puromycin selection were expanded and analyzed by Southern blot to confirm recombinant ES clones. After BamHI digestion, the bands representing WT and mutant alleles are 9.0 and 6.8 kb, respectively. Targeted ES cells were selected for microinjection into C57BL/6 blastocysts to generate chimeras. The male chimeras were bred with C57BL/6 female mice to select for germline transmission. To remove the puromycin selection cassette, targeted heterozygous F1 was crossed with Flp deleter strain (FLPeR mice, The Jackson Laboratory strain 003946). The mice were backcrossed to C57BL/6 then crossed with Alb-Cre mice (The Jackson Laboratory strain 003574) to generate liver-specific Ror α -deficient mice. Male ROR $\alpha^{fl/fl}$ and ROR α^{LKO} mice at 8 weeks of age were fed a CD or a 60% kcal fat HFD (Research diet, D12492) during 10 weeks. The sample sizes for all animal studies were announced in each figure legend. Mice were housed in a specific pathogen-free AAALAC-accredited facility under controlled conditions of temperature (25 °C) and light (12 h light:12 h dark, lights switched on at 7:00 a.m.). Food and water were available ad libitum. All mice used in these experiments were backcrossed to C57BL/6 at least seven generations. Animals for each group of experiments were chosen randomly. The primers used in PCR analysis for genotyping floxed alleles are: forward 5'-GCTTGTGGGTTTCTCTACA-3' and reverse 5'-GCAGCAAGTGTGTGCCCA-3'. This study was reviewed and approved by the Institutional Animal Care and Use Committee (IACUC) of National Cancer Center Research Institute.

Body composition. Fat and lean body masses were assessed by ^1H magnetic resonance spectroscopy (Bruker BioSpin).

Indirect calorimetry. Oxygen consumption (VO_2), carbon dioxide production (VCO_2), respiratory exchange ratios, EE and food consumption were measured using an indirect calorimetry system PHENOMASTER (TSE System). Mice in each chamber were maintained at a constant environmental temperature of 22 °C.

Isolation and culture of primary mouse hepatocytes. Mouse primary hepatocytes were isolated from the liver of 8-week-old male ROR $\alpha^{fl/fl}$ and ROR α^{LKO} mice or WT and PPAR α null mice by the collagenase perfusion method⁶⁵. Dissociation into individual hepatocytes was performed in Dulbecco's modified Eagles' medium (DMEM) (Wegene) containing 10% heat-inactivated fetal bovine serum (FBS), 1% antibiotics, 20 mM HEPES, 100 nM insulin, 1 nM dexamethasone. For each hepatocyte preparation, cell viability was estimated by the exclusion of trypan blue.

Total bile acid (TBA) measurement. The quantitative determination of total bile acid of mice serum that was collected after centrifugation of mice blood was measured using the total bile acids assay kit (DZ042A-K, Diazyme Laboratories), according to the manufacturer's instructions.

Histology. When mice were euthanized by CO_2 asphyxiation, livers and white adipose tissues (WATs) were rapidly fixed in 10% formalin (Sigma) at 4 °C overnight. After fixation, tissues were sequentially dehydrated in ethanol with increasing concentrations ranging from 50 to 100%. Dehydrated specimens were subsequently infiltrated with 100% xylene and embedded in paraffin wax. For hematoxylin and eosin (H&E) staining, tissues were sectioned at 5 μm thickness, deparaffinized, rehydrated and stained with hematoxylin for 3 min followed by counterstaining with eosin for 1 min. For Oil red O staining, fresh samples of liver embedded in OCT tissue freezing medium (Sakura Finetek), 0.5% Oil red O solution was prepared by dissolving 0.5 g Oil red O powder (Sigma) in 100 ml propylene glycol (sigma). Fresh frozen specimens were cryosectioned at 8 μm thickness and air dried. Then fix in ice cold 10% formalin for 10 min, air dried again, and rinsed with distilled water. Sections were placed in 100% propylene glycol for 5 min and stained with pre-warmed 0.5% Oil red O solution in propylene glycol for 15 min in 60 °C oven. Then sections were rinsed with distilled water and followed by counterstaining with hematoxylin. Images were acquired using digital microscopes (Leica DMD108, Leica microsystems) equipped with $\times 10$ and $\times 20$ objective lenses.

Quantitative real-time RT-PCR. Total RNAs were extracted using Trizol (Invitrogen) and reverse transcription was performed from 2.5 μg of total RNAs using the M-MLV cDNA Synthesis kit (Enzymomics). The abundance of mRNA was detected by a CFX384 TouchTM Real-Time PCR Detection System (Bio-Rad) with SYBR Green (Enzymomics). The quantity of mRNA was calculated using $\Delta\Delta\text{Ct}$ method and normalized by using primers indicated in each figure legend. All reactions were performed as triplicates. Primers used for analysis are listed in Supplementary Data 5.

Intraperitoneal glucose or insulin tolerance tests. For GTTs, 2 g of glucose per kg of mice body weight was injected i.p. to overnight fasted mice. For ITTs, 0.75 U of insulin (Humulin R, Eli Lilly) per kg of mice body weight was injected i.p. to 6 h fasted mice. Mice blood was drawn at indicated time intervals from the tail tip puncture, and blood glucose level was measured by accu-check performa glucometer (Roche).

Generation of mRNA-sequencing data. Four groups of mice, CD-fed ROR $\alpha^{fl/fl}$, CD-fed ROR α^{LKO} , HFD-fed ROR $\alpha^{fl/fl}$ and HFD-fed ROR α^{LKO} mice, were analyzed by RNA-sequencing. Four mice per group were killed, and livers from two mice were pooled to generate two samples per group, that is, duplicate experiments for each group were performed. Total RNA extraction was performed using Trizol (Invitrogen). Poly(A) mRNA isolation from total RNA and fragmentation were performed using the Illumina Truseq RNA Sample Prep Kit with poly-T oligo-attached magnetic beads, according to the manufacturer's instructions. Reverse transcription of RNA fragments was performed using Superscript II reverse transcriptase (Life Technologies). The adaptor-ligated library was size-selected by band excision after agarose gel electrophoresis and purified using the QIAquick gel extraction kit (Qiagen). The prepared mRNA-sequencing libraries were pair-end sequenced on an Illumina Hi-seq 2500. The accession number for the mRNA-sequencing data in this paper is GSE83338.

Analysis of mRNA-sequencing data. After removing adapter sequences (TrueSeq universal and index adapters), we used cutadapter software⁶⁶ to trim the reads that PHRED scores lower than 20. Remaining reads were aligned to the mouse reference genome (GRCm38) using TopHat aligner⁶⁷. After the alignment, we quantified the expression of genes as Fragments Per Kilobase of transcript per Million mapped reads (FPKM) for each gene using Cufflinks⁶⁸. To identify the DEGs, we first selected the 'expressed' genes as the ones with FPKM larger than 1 under at least one of the eight samples. For the expressed genes, $\log_2(\text{FPKM} + 1)$ values were normalized across eight samples using the quantile normalization method. To identify the DEGs, for each gene, we calculated a T-statistic and \log_2 -fold-change in the comparisons of ROR $\alpha^{LKO}/\text{ROR}\alpha^{fl/fl}_{\text{HFD}}$ and ROR $\alpha^{LKO}/\text{ROR}\alpha^{fl/fl}_{\text{CD}}$. We then estimated empirical distributions of T-statistics and \log_2 -fold changes for the null hypothesis by random permutation of the eight samples (1000 permutations). On the basis of the distributions, for each gene, we computed adjusted P values for the observed T-statistic and \log_2 -fold-change and the combined these P values with Stouffer's method⁶⁹. Finally, we identified the DEGs as the ones that have the combined P-value ≤ 0.05 and absolute \log_2 -fold-change ≥ 0.439 , which is a cutoff value (the 95th percentile of the empirical distribution for \log_2 -fold changes) for each comparison. We further identified ROR α -dependent genes under HFD condition as the ones with significant differences between the \log_2 -fold-change in the two comparisons above (ROR $\alpha^{LKO}/\text{ROR}\alpha^{fl/fl}_{\text{HFD}}$ and ROR $\alpha^{LKO}/\text{ROR}\alpha^{fl/fl}_{\text{CD}}$) larger than 0.439.

Functional enrichment analysis and TF enrichment analysis. For the genes in Groups 1–8, enrichment analysis of GOBPs and KEGG pathways were performed using a DAVID software³⁴. We selected the GOBPs and KEGG pathways with P-value < 0.05 as the ones represented by the genes analyzed. For the genes in Group 1, TF enrichment analysis was performed using a ChEA2 software³³. Among the TF-target gene data, only mouse TF-target gene data were used for the enrichment analysis. We selected the TFs with P-value < 0.01 as the ones significantly regulating the genes in Group 1.

Luciferase reporter assay. HEK293T cells (ATCC) and Hep3B cells (Korean Cell Line Bank) were grown and transiently transfected by using polyethylenimine (PEI) and turbofect (Thermo Scientific, R0531). All cell lines used in the study were regularly tested for mycoplasma contamination. For luciferase reporter assays, 1×10^5 cells were seeded in DMEM supplemented with 10% FBS and 1% antibiotics. Cells were transfected with PPRE-luciferase reporters and β -galactosidase expression constructs along with several expression constructs were indicated in each figure. Using a luciferase assay system (Promega), the luciferase activity was measured with a luminometer (Berthold Technologies) after 48 h of transfection. Transfection efficiency was normalized by β -galactosidase expression. The results were obtained from at least three independent experiments

Co-immunoprecipitation assay. HEK293T cells that transfected with Flag-HDACs and HA-ROR α were cultured and lysed with lysis buffer (200 mM NaCl, 50 mM Tris-HCl, pH 8.0 and 0.5% NP40). About 20 mg of cell extracts was

immunoprecipitated with each 1 µg of anti-Flag antibody overnight and then incubated with 35 µl (50% slurry) of protein A/G agarose beads for 1 h. The immunoprecipitated materials were washed with 500 µl of washing buffer (150 mM NaCl, 50 mM Tris-HCl, pH 8.0 and 0.5% NP40) for four times and bound materials were eluted by boiling in 50 µl of sampling buffer (2% β-mercaptoethanol, 5% glycerol, 1% SDS and 60 mM Tris-HCl, pH 6.8) and subjected to immunoblot analysis. Protein samples were resolved by sodium dodecyl sulphate-polyacrylamide gel electrophoresis. Images of the immunoblots were visualized and recorded using the LAS 4000-mini system (Fujifilm). Original uncropped images of immunoblots used in this study can be found in Supplementary Fig. 8.

Chromatin Immunoprecipitation (ChIP) and Re-ChIP assays. The ChIP assays were conducted as described. Cells were crosslinked with 1% formaldehyde for 10 min at room temperature. Mouse livers were harvested and quickly washed with PBS and crosslinked with 1% formaldehyde for 10 min at room temperature, followed by quenching with 0.125 M glycine solution for 5 min. Then, cells or harvested mouse livers were washed with ice-cold PBS two times. Chromatin fragmentation was performed by sonication in ChIP lysis buffer (50 mM Tris-HCl (pH 8.1), 1% SDS, 10 mM EDTA (pH 7.6), and protease inhibitor cocktail) with an average size of approximately 500 bp. Proteins were immunoprecipitated in ChIP dilution buffer (1% Triton X-100, 2 mM EDTA, 150 mM NaCl, 20 mM Tris-HCl (pH 8.1), and protease inhibitor cocktail). Crosslinking was reversed overnight at 65 °C in elution buffer (1% SDS, 0.1 M NaHCO₃), and DNA was purified with a QIAquick Gel extraction Kit (QIAGEN). For the Re-ChIP assay, components were eluted from the first immunoprecipitation reaction by incubation with 10 mM DTT at 37 °C for 30 min and diluted 1:50 with ChIP dilution buffer containing 20 mM Tris-HCl (pH 8.1), 150 mM NaCl, 2 mM EDTA, and 1% Triton X-100 followed by reimmunoprecipitation with the secondary antibody. Precipitated DNA was analyzed by quantitative PCR. For real-time quantitative PCR analysis, 2 µl from 60 µl DNA extractions was used. All reactions were performed in triplicates. Primers used for analysis are listed in Supplementary Data 5.

GW9662-treated mice. ROR^{fl/fl} and ROR^α^{LKO} male mice at 8 weeks of age were subjected to GW9662 at a dose of 0.35 mg per kg body weight per day or an equivalence volume of vehicle in their drinking water for 5 weeks with feeding HFD. The sample sizes for this study was announced in figure legend.

Antibodies. Commercially available antibodies were used: anti-ROR^α (sc-28612; 1:1000 dilution for IB analysis, 5 µg for ChIP assay), anti-tubulin (sc-8035, 1:5000 dilution for IB analysis), anti-AKT (sc-8312; 1:1000 dilution for IB analysis), anti-PPAR^α (sc-9000x, 1 µg for ChIP assay) and anti-GFP (sc-9996, 1 µg for ChIP assay) from Santa Cruz Biotechnology; anti-β-actin (A5441; 1:5000 dilution for IB analysis) and anti-FLAG (F3165, Sigma, 1:5000 dilution for IB analysis, 1 µg for IP assay) from Sigma; anti-HA (MMS-101R; 1:5000 dilution for IB analysis, 1 µg for IP assay) from Covance; anti-H3Ac (#06-599, 1 µg for ChIP assay) from Millipore; anti-phospho-AKT(Ser473) (#4051 S, 1:1000 dilution for IB analysis) from Cell Signaling; anti-PPAR^γ (ab41928, 1 µg for ChIP assay), anti-PGC1^α (ab54481, 1 µg for ChIP assay) and anti-HDAC3 (ab7030, 1 µg for ChIP assay) from Abcam; anti-RNA polymerase II (MMS-126R, 1 µg for ChIP assay) from Berkeley antibody company; anti-V5 (R96025; 1:5000 dilution for IB analysis) from Invitrogen.

Statistical analysis. For animal studies, sample size for experiments were determined empirically based on previous studies to ensure appropriate statistical power. Animals for each group of experiments were chosen randomly. No animals were excluded from statistical analysis, and the investigators were not blinded in the studies. The statistical analysis of different groups is realized using the Student's unpaired *t*-test or one-way analysis of variance (ANOVA) followed by Tukey post hoc test or two-way ANOVA. SPSS software (IBM) was used for all analyses.

Data availability. mRNA-sequencing data that support the findings of this study have been deposited in Gene Expression Omnibus (GEO) with the primary accession codes GSE83338.

Received: 6 October 2016 Accepted: 9 June 2017

Published online: 31 July 2017

References

- Despres, J. P. & Lemieux, I. Abdominal obesity and metabolic syndrome. *Nature* **444**, 881–887 (2006).
- Van Gaal, L. F., Mertens, I. L. & De Block, C. E. Mechanisms linking obesity with cardiovascular disease. *Nature* **444**, 875–880 (2006).
- Heymsfield, S. B. & Wadden, T. A. Mechanisms, pathophysiology, and management of obesity. *N. Engl. J. Med.* **376**, 254–266 (2017).
- Rutkowski, J. M., Stern, J. H. & Scherer, P. E. The cell biology of fat expansion. *J. Cell Biol.* **208**, 501–512 (2015).
- van den Berghe, G. The role of the liver in metabolic homeostasis: implications for inborn errors of metabolism. *J. Inher. Metab. Dis.* **14**, 407–420 (1991).
- Browning, J. D. & Horton, J. D. Molecular mediators of hepatic steatosis and liver injury. *J. Clin. Invest.* **114**, 147–152 (2004).
- Samuel, V. T. et al. Mechanism of hepatic insulin resistance in non-alcoholic fatty liver disease. *J. Biol. Chem.* **279**, 32345–32353 (2004).
- Chawla, A. et al. A PPAR gamma-LXR-ABCA1 pathway in macrophages is involved in cholesterol efflux and atherogenesis. *Mol. Cell* **7**, 161–171 (2001).
- Giguere, V. Orphan nuclear receptors: from gene to function. *Endocr. Rev.* **20**, 689–725 (1999).
- Baek, S. H. & Kim, K. I. Emerging roles of orphan nuclear receptors in cancer. *Annu. Rev. Physiol.* **76**, 177–195 (2014).
- Bookout, A. L. et al. Anatomical profiling of nuclear receptor expression reveals a hierarchical transcriptional network. *Cell* **126**, 789–799 (2006).
- Mullican, S. E., Dispirito, J. R. & Lazar, M. A. The orphan nuclear receptors at their 25-year reunion. *J. Mol. Endocrinol.* **51**, T115–140 (2013).
- Pearen, M. A. & Muscat, G. E. Orphan nuclear receptors and the regulation of nutrient metabolism: understanding obesity. *Physiology (Bethesda)* **27**, 156–166 (2012).
- Li, L. et al. The nuclear orphan receptor COUP-TFII plays an essential role in adipogenesis, glucose homeostasis, and energy metabolism. *Cell Metab.* **9**, 77–87 (2009).
- Kim, D. K. et al. Orphan nuclear receptor estrogen-related receptor gamma (ERRgamma) is key regulator of hepatic gluconeogenesis. *J. Biol. Chem.* **287**, 21628–21639 (2012).
- Ranhotra, H. S. The orphan nuclear receptors in cancer and diabetes. *J. Recept. Signal. Transduct. Res.* **33**, 207–212 (2013).
- Pellicciari, R. et al. 6alpha-ethyl-chenodeoxycholic acid (6-ECDC), a potent and selective FXR agonist endowed with anticholestatic activity. *J. Med. Chem.* **45**, 3569–3572 (2002).
- Billin, A. N. PPAR-beta/delta agonists for Type 2 diabetes and dyslipidemia: an adopted orphan still looking for a home. *Expert. Opin. Investig. Drugs* **17**, 1465–1471 (2008).
- Katz, A. et al. Safety, pharmacokinetics, and pharmacodynamics of single doses of LXR-623, a novel liver X-receptor agonist, in healthy participants. *J. Clin. Pharmacol.* **49**, 643–649 (2009).
- Lee, J. M. et al. RORalpha attenuates Wnt/beta-catenin signaling by PKCalpha-dependent phosphorylation in colon cancer. *Mol. Cell* **37**, 183–195 (2010).
- Kim, H. et al. DNA damage-induced RORalpha is crucial for p53 stabilization and increased apoptosis. *Mol. Cell* **44**, 797–810 (2011).
- Vogel, M. W., Sinclair, M., Qiu, D. & Fan, H. Purkinje cell fate in staggerer mutants: agenesis versus cell death. *J. Neurobiol.* **42**, 323–337 (2000).
- Doulazmi, M. et al. Cerebellar Purkinje cell loss during life span of the heterozygous staggerer mouse (Rora(+)/Rora(sg)) is gender-related. *J. Comp. Neurol.* **411**, 267–273 (1999).
- Guillaumond, F., Dardente, H., Giguere, V. & Cermakian, N. Differential control of Bmal1 circadian transcription by REV-ERB and ROR nuclear receptors. *J. Biol. Rhythms* **20**, 391–403 (2005).
- Sato, T. K. et al. A functional genomics strategy reveals Rora as a component of the mammalian circadian clock. *Neuron* **43**, 527–537 (2004).
- Vu-Dac, N. et al. Transcriptional regulation of apolipoprotein A-I gene expression by the nuclear receptor RORalpha. *J. Biol. Chem.* **272**, 22401–22404 (1997).
- Mamontova, A. et al. Severe atherosclerosis and hypoalphalipoproteinemia in the staggerer mouse, a mutant of the nuclear receptor RORalpha. *Circulation* **98**, 2738–2743 (1998).
- Lau, P. et al. The orphan nuclear receptor, RORalpha, regulates gene expression that controls lipid metabolism: staggerer (SG/SG) mice are resistant to diet-induced obesity. *J. Biol. Chem.* **283**, 18411–18421 (2008).
- Watanabe, M. et al. Bile acids induce energy expenditure by promoting intracellular thyroid hormone activation. *Nature* **439**, 484–489 (2006).
- Kahn, B. B. & Flier, J. S. Obesity and insulin resistance. *J. Clin. Invest.* **106**, 473–481 (2000).
- Wolfrum, C., Asilmaz, E., Luca, E., Friedman, J. M. & Stoffel, M. Foxa2 regulates lipid metabolism and ketogenesis in the liver during fasting and in diabetes. *Nature* **432**, 1027–1032 (2004).
- Moller, D. E. & Kaufman, K. D. Metabolic syndrome: a clinical and molecular perspective. *Annu. Rev. Med.* **56**, 45–62 (2005).
- Huang da, W., Sherman, B. T. & Lempicki, R. A. Bioinformatics enrichment tools: paths toward the comprehensive functional analysis of large gene lists. *Nucleic Acids Res.* **37**, 1–13 (2009).
- Huang da, W., Sherman, B. T. & Lempicki, R. A. Systematic and integrative analysis of large gene lists using DAVID bioinformatics resources. *Nat. Protoc.* **4**, 44–57 (2009).
- Kou, Y. et al. ChEA2: gene-set libraries from ChIP-X experiments to decode the transcription regulome. Multidisciplinary research and practice for information systems. CD-ARES 2013. *Lect. Notes Comput.* **8127**, 416–430 (2013).

36. Dreyer, C. et al. Control of the peroxisomal beta-oxidation pathway by a novel family of nuclear hormone receptors. *Cell* **68**, 879–887 (1992).
37. Lee, J. M. et al. Nutrient-sensing nuclear receptors coordinate autophagy. *Nature* **516**, 112–115 (2014).
38. Kersten, S. et al. Peroxisome proliferator-activated receptor alpha mediates the adaptive response to fasting. *J. Clin. Invest.* **103**, 1489–1498 (1999).
39. Puigserver, P. & Spiegelman, B. M. Peroxisome proliferator-activated receptor-gamma coactivator 1 alpha (PGC-1 alpha): transcriptional coactivator and metabolic regulator. *Endocr. Rev.* **24**, 78–90 (2003).
40. Hong, H., Kohli, K., Trivedi, A., Johnson, D. L. & Stallcup, M. R. GRIP1, a novel mouse protein that serves as a transcriptional coactivator in yeast for the hormone binding domains of steroid receptors. *Proc. Natl Acad. Sci. USA* **93**, 4948–4952 (1996).
41. Wagner, M., Zollner, G. & Trauner, M. Nuclear receptors in liver disease. *Hepatology* **53**, 1023–1034 (2011).
42. Nakano, R. et al. Antagonism of peroxisome proliferator-activated receptor gamma prevents high-fat diet-induced obesity in vivo. *Biochem. Pharmacol.* **72**, 42–52 (2006).
43. Ma, S. et al. Thyrotropin and obesity: increased adipose triglyceride content through glycerol-3-phosphate acyltransferase 3. *Sci. Rep.* **5**, 7633 (2015).
44. Ye, J. M. et al. Direct demonstration of lipid sequestration as a mechanism by which rosiglitazone prevents fatty-acid-induced insulin resistance in the rat: comparison with metformin. *Diabetologia* **47**, 1306–1313 (2004).
45. Kim, J. K. et al. Differential effects of rosiglitazone on skeletal muscle and liver insulin resistance in A-ZIP/F-1 fatless mice. *Diabetes* **52**, 1311–1318 (2003).
46. Auwerx, J. PPARgamma, the ultimate thrifty gene. *Diabetologia* **42**, 1033–1049 (1999).
47. Sirtori, A. R. & Olefsky, J. M. Thiazolidinediones in the treatment of insulin resistance and type II diabetes. *Diabetes* **45**, 1661–1669 (1996).
48. Way, J. M. et al. Comprehensive messenger ribonucleic acid profiling reveals that peroxisome proliferator-activated receptor gamma activation has coordinate effects on gene expression in multiple insulin-sensitive tissues. *Endocrinology* **142**, 1269–1277 (2001).
49. Schadinger, S. E., Bucher, N. L., Schreiber, B. M. & Farmer, S. R. PPARgamma2 regulates lipogenesis and lipid accumulation in steatotic hepatocytes. *Am. J. Physiol. Endocrinol. Metab.* **288**, E1195–E1205 (2005).
50. Lee, Y. J. et al. Nuclear receptor PPARgamma-regulated monoacylglycerol O-acyltransferase 1 (MGAT1) expression is responsible for the lipid accumulation in diet-induced hepatic steatosis. *Proc. Natl. Acad. Sci. USA* **109**, 13656–13661 (2012).
51. Vidal-Puig, A. et al. Regulation of PPAR gamma gene expression by nutrition and obesity in rodents. *J. Clin. Invest.* **97**, 2553–2561 (1996).
52. Yu, S. et al. Adipocyte-specific gene expression and adipogenic steatosis in the mouse liver due to peroxisome proliferator-activated receptor gamma1 (PPARgamma1) overexpression. *J. Biol. Chem.* **278**, 498–505 (2003).
53. Yamauchi, T. et al. Inhibition of RXR and PPARgamma ameliorates diet-induced obesity and type 2 diabetes. *J. Clin. Invest.* **108**, 1001–1013 (2001).
54. Matusue, K. et al. Liver-specific disruption of PPARgamma in leptin-deficient mice improves fatty liver but aggravates diabetic phenotypes. *J. Clin. Invest.* **111**, 737–747 (2003).
55. Choi, S. S. et al. PPARgamma antagonist gleevec improves insulin sensitivity and promotes the browning of white adipose tissue. *Diabetes* **65**, 829–839 (2016).
56. Moran-Salvador, E. et al. Role for PPARgamma in obesity-induced hepatic steatosis as determined by hepatocyte- and macrophage-specific conditional knockouts. *FASEB J.* **25**, 2538–2550 (2011).
57. Hashimoto, T. et al. Defect in peroxisome proliferator-activated receptor alpha-inducible fatty acid oxidation determines the severity of hepatic steatosis in response to fasting. *J. Biol. Chem.* **275**, 28918–28928 (2000).
58. Ohoka, N., Kato, S., Takahashi, Y., Hayashi, H. & Sato, R. The orphan nuclear receptor RORalpha restrains adipocyte differentiation through a reduction of C/EBPbeta activity and perilipin gene expression. *Mol. Endocrinol.* **23**, 759–771 (2009).
59. Kliewer, S. A., Umesono, K., Noonan, D. J., Heyman, R. A. & Evans, R. M. Convergence of 9-cis retinoic acid and peroxisome proliferator signalling pathways through heterodimer formation of their receptors. *Nature* **358**, 771–774 (1992).
60. Palmer, C. N., Hsu, M. H., Griffin, H. J. & Johnson, E. F. Novel sequence determinants in peroxisome proliferator signaling. *J. Biol. Chem.* **270**, 16114–16121 (1995).
61. Harding, H. P. & Lazar, M. A. The monomer-binding orphan receptor Rev-Erb represses transcription as a dimer on a novel direct repeat. *Mol. Cell Biol.* **15**, 4791–4802 (1995).
62. Sun, Z. et al. Deacetylase-independent function of HDAC3 in transcription and metabolism requires nuclear receptor corepressor. *Mol. Cell* **52**, 769–782 (2013).
63. Sun, Z. et al. Hepatic Hdac3 promotes gluconeogenesis by repressing lipid synthesis and sequestration. *Nat. Med.* **18**, 934–942 (2012).
64. Lau, P., Fitzsimmons, R. L., Pearen, M. A., Watt, M. J. & Muscat, G. E. Homozygous staggerer (sg/sg) mice display improved insulin sensitivity and enhanced glucose uptake in skeletal muscle. *Diabetologia* **54**, 1169–1180 (2011).
65. Kang, H. S. et al. Metformin stimulates IGF2 gene expression through PPARalpha in diabetic states. *Sci. Rep.* **6**, 23665 (2016).
66. Martin, M. Cutadapt removes adapter sequences from high-throughput sequencing reads. *EMBnet J.* **17**, 10–12 (2011).
67. Trapnell, C., Pachter, L. & Salzberg, S. L. TopHat: discovering splice junctions with RNA-Seq. *Bioinformatics* **25**, 1105–1111 (2009).
68. Trapnell, C. et al. Transcript assembly and quantification by RNA-Seq reveals unannotated transcripts and isoform switching during cell differentiation. *Nat. Biotechnol.* **28**, 511–515 (2010).
69. Hwang, D. et al. A data integration methodology for systems biology. *Proc. Natl Acad. Sci. USA* **102**, 17296–17301 (2005).

Acknowledgements

We thank members of the Chromatin Dynamics Research Center for technical assistance and discussions, J.B.K. for providing PPARy constructs. We thank the NCC Animal Sciences Branch for excellent guidance and assistance with the performed mouse experiments. This work was supported by Creative Research Initiatives Program (Research Center for Chromatin Dynamics, 2009-0081563) to S.H.B.; Global PH.D Fellowship Program (NRF-2011-0008101) to K.K. and (NRF-2012H1A2A1009905) to Y.S.Y.; Korea Mouse Phenotyping Project (2013M3A9D5072550) to S.G.Y., I.Y.K., J.K.S. and S.F.; Basic Science Research Program (NRF-2015R1D1A1A01058037) to K.B., (NRF-2014R1A6A3A04057910) to H.K.; and (NRF-2015R1C1A1A01052195) to S.F.; Medical Research Center (NRF-2014R1A5A2010008) to S.-S.I.; Institute for Basic Science (IBS-R013-G1) to D.H. from the National Research Foundation (NRF) grant funded by the Korea government (MSIP). H.L. was supported by the National Cancer Center Grant (NCC-1310100).

Author contributions

K.K., K.I.K., H.L., S.F. and S.H.B. designed the experiments. K.K., K.B., S.K.O. Y.J. and H.L. generated and maintained ROR $\alpha^{fl/fl}$ and ROR α^{LKO} mice. S.G.Y., I.Y.K. and J.K.S. performed mouse metabolic cage assay. J.-S.L. and S.-S.I. provided Ppara-null primary hepatocyte. K.K., S.K.O. and S.F. analyzed mouse phenotype. K.K. performed histological assays. K.K., K.B., S.K.O. and H.K. performed the cell biology and biochemistry experiments. K.K., Y.S.Y., J.B. and D.H. performed mRNA-sequencing preparation and analysis. K.K., Y.S.Y., D.H., S.F. and S.H.B. wrote the manuscript. All authors contributed to data analysis.

Additional information

Supplementary Information accompanies this paper at doi:10.1038/s41467-017-00215-1.

Competing interests: The authors declare no competing financial interests.

Reprints and permission information is available online at <http://npg.nature.com/reprintsandpermissions/>

Publisher's note: Springer Nature remains neutral with regard to jurisdictional claims in published maps and institutional affiliations.



Open Access This article is licensed under a Creative Commons Attribution 4.0 International License, which permits use, sharing, adaptation, distribution and reproduction in any medium or format, as long as you give appropriate credit to the original author(s) and the source, provide a link to the Creative Commons license, and indicate if changes were made. The images or other third party material in this article are included in the article's Creative Commons license, unless indicated otherwise in a credit line to the material. If material is not included in the article's Creative Commons license and your intended use is not permitted by statutory regulation or exceeds the permitted use, you will need to obtain permission directly from the copyright holder. To view a copy of this license, visit <http://creativecommons.org/licenses/by/4.0/>.

© The Author(s) 2017